Dynamic Compaction of a Thin Subgrade Layer Overlying Weak Deposit

Mustafa Yulek

A Thesis

in

The Department

of

Building, Civil and Environmental Engineering

Presented in Partial Fulfillment of the Requirements

For the Degree of Master of Applied Science at

Concordia University

Montreal, Quebec, CANADA

April 2006

Your file Votre référence
ISBN: 0-494-14250-2
Our file Notre référence
ISBN: 0-494-14250-2

ABSTRACT

Dynamic Compaction of a Thin Subgrade Layer Overlying Weak Deposit

Mustafa Yulek

Dynamic Compaction of soils is a wide-spread soil improvement technique that has been used with proven effectiveness in the field of Geotechnical Engineering. It is performed by dropping a given weight from a specified height on the ground. The produced energy transmits compression waves through the soil layers, which generates vibrations causing the densification of the soil particles. The technique is environmentally friendly and simple to apply, which enabled geotechnical engineers to consider it as one of the primary solutions for densification of weak soil encountered in construction of foundation, highways and embankment.

Despite the latest developments in technology and equipment, roads and highways suffer from poor compaction of subgrade material supporting the pavement layer. Subsequently, degradation of the subgrade material occurs and the situation offers low serviceability and high maintenance costs for highways. The problem stated comprises a major difficulty in the construction of these projects.

Field compaction is controlled by the results of the laboratory test known as "Proctor test". Quite often field compaction does not match the results produced from the laboratory test. This is due to the fact that the field boundary conditions are not compatible with those of the laboratory test. Therefore, the existence of a weak deposit underlying the thin subgrade layer influences the compaction level to a great extent.

Accordingly, Proctor values sometimes are misleading in predicting the level of compaction that could be attained in the field.

This thesis presents an axisymmetric numerical model to simulate Dynamic Compaction of a thin subgrade layer overlying a deep deposit of various stiffness levels. The compaction effort is applied by means of impact energy on the ground and modeled as a transient loading having a constant frequency level with different amplitude values depending on the energy level used. On the light of the numerical model results obtained, it can be reported that the presence of weak deposit significantly affects the compaction level of the subgrade. The results depend on the thickness of the subgrade layer, stiffness of the underlying deposit and the energy level used. The energy consumed to compact the subgrade layer and further the energy dissipated to the lower deposit were measured, and accordingly, the level of compaction for a given soil/load/geometry conditions was predicted. Design procedure was given for practicing use. Designer may consider alternatives for undesirable cases such to improve the lower layer before compaction using other methods of soil improvement.

ACKNOWLEDGEMENTS

I would like to take this opportunity to express my sincere gratitude to my supervisor, Dr. Hanna, for his continuous support and encouragement throughout my graduate studies and for being more than a supervisor to me.

Many thanks go to a very good friend, Dr. Mohab Sabry for his valuable discussions on this research we had in the late night hours at the ER-303 Computer Lab.

Being far away from them would only make me stronger with their prayers; I would like to dedicate all the effort, hard work and fun of this study to my father and my mother, Ali & Hatice Yulek.

Mustafa Yulek

TABLE OF CONTENTS

LIST OF SYMBOLS

Symbols

d_{max}	=	Depth of improvement
λ	=	Empirical coefficient for energy per drop
W	=	Weight of tamper
H	=	Drop height
g	=	Gravitational constant
F_{max}	=	Peak dynamic force
Δt	=	Total time for deceleration
m	=	Mass of tamper
Δv	=	Change in velocity
a_{max}	=	peak deceleration
f_n	=	Natural frequency of a system
T	=	Period of vibration
k	=	Vertical stiffness of the system
G	=	Shear modulus
r_o	=	Radius of the tamper
ν	=	Poisson's ratio
A_p	=	Base area of the tamper
G_{max}	=	Dynamic shear modulus at high strain levels
Ip	=	Plasticity index of soil
γ	=	Strain level
ρ	=	Density

Vs	=	Shear wave velocity
M	=	Oedometer modulus
E	=	Elasticity modulus
α	=	Rayleigh damping parameter for mass
β	=	Rayleigh damping parameter for stiffness
γ_{unsat}	=	Unsaturated unit weight
γ_{sat}	=	Saturated unit weight
k_x	=	Horizontal permeability coefficient
k_y	=	Vertical permeability coefficient
C	=	Cohesion
Φ	=	Internal friction angle
[C]	=	Rayleigh damping matrix of the system
[M]	=	Mass matrix of the system
[K]	=	Stiffness matrix of the system
D	=	Material damping ratio
ω	=	Circular frequency
EL	=	Energy level per drop
e	=	Void ratio
x	=	Vertical deformation of the spring
EN_1	=	Energy absorbed by the subgrade
EN_2	=	Energy absorbed by lower layer
$EN_{resisted}$	=	Resisted energy by lower layer
Ts	=	Thickness of the subgrade layer

R^2	=	Coefficient of determination
a, b, c	=	Coefficients for energy dissipation to the lower layer
a(y)	=	Vertical acceleration
γ_{dry}	=	Dry unit weight
$\gamma_{proctor}$	=	Proctor dry unit weight
$\gamma_{initial}$	=	Dry unit weight before compaction

LIST OF FIGURES

LIST OF TABLES

Description **Page**

CHAPTER 1

INTRODUCTION

1.1 GENERAL

Compaction of ground is a soil improvement technique which has been used widely in the field of geotechnical engineering. The weak conditions of the ground through visual inspection have directed civil engineering to compact the ground using the available heavy equipment. With emerging technologies and better understanding of soil mechanics, compaction of ground has become a primary solution to weak soils encountered in the field as soil improvement for foundation, highway and embankment. The primary objective of compaction was to improve the bearing capacity of the foundation and to enhance settlement characteristics. Compaction was then known as the process to expel air and fluids from the void space by means of applying mechanical energy. Nevertheless, no theories were available to estimate the energy level needed and the result expected.

Due to the recent development of equipments and technologies, compaction became wide-spread as a vital soil improvement technique. Good results were achieved in case of a thin subgrade layer overlying a deep strong deposit. However, the level of compaction achieved may vary significantly in case of the deposit was made of weak material; depending on the strength of the deposit the level of compaction achieved may vary zero to 100% of the Proctor value.

1.2 PROBLEM STATEMENT

The degradation of the condition of Roads and highways in North America are mainly due to the poor compaction of the subgrade material, which supports the pavement layer. This thesis presents a numerical model to simulate the case of a thin subgrade layer overlying a deep deposit. The subgrade layer will be subjected to dynamic loading for a specified energy level. The produced unit weight of the subgrade layer as a result of the compaction process will be compared to the Proctor value on the light of the shear strength of the deposit. In this research it is intended to develop a theory to correlate the energy consumed to the strength of the deposit for a given thickness of the subgrade layer.

1.2.1 BOUNDARY CONDITIONS OF THE PROBLEM

When the compaction effort is applied onto the soil, the energy is distributed along the soil particles and attenuates through geometric and material damping in case of a homogenous soil to an infinite depth. However, when boundary conditions exist, the generated energy to execute the compaction process is reflected or absorbed to some extent with respect to the energy level, depth to the boundary and the mechanical properties of the material beyond this boundary. When a subgrade layer is subjected to compaction, the energy waves are distributed through the target layer to the interface of the underlying layer. Depending on the shear strength of the underlying layer, the energy waves may seep through or be will reflected in full or in part. The portion of the wave energy, which will be reflected back to the subgrade layer, will be responsible of its compaction. Accordingly, in case of a soft layer underlying the subgrade layer, the

energy will dissipate entirely to the soft layer, causing no compaction to the subgrade layer.

1.3 DYNAMIC COMPACTION METHOD

Dynamic Compaction is one of the widely used ground improvement techniques available to the engineers today. It is particularly efficient in case of loose unsaturated granular soils. It has also been used successfully on cohesive soils of high void ratio, and on wastes and fills (Pan and Selby, 2002). The main objective of using dynamic compaction is to achieve densification by means of applying highly localized impact energy onto the ground, which will cause physical displacement of particles and low frequency excitation in the range of 2 to 20 Hz. This procedure will reduce the void ratio of soil, and accordingly, it will increase the relative density, and further improve the bearing capacity and settlement characteristics of the foundation. Dynamic compaction has been used successfully for a variety of civil engineering projects such as buildings, airports, highways and to reduce liquefaction potential of loose soils.

Dynamic compaction is carried out by the dropping of heavy weights onto the ground in a grid pattern. The weight, which is often referred to as "tamper", is typically made of steel or reinforced concrete. As reported by Kerisel (1985), the Romans have used similar technique for construction purposes and Lundwall (1968) also reported that an old war cannon was used to compact ground in 1871 (Scolombe, 1993). In the twentieth century compaction has been provided to an airport in China, a port area in Dublin during the 1940's, and to oil tank in South Africa in 1955. However, the advent of

large crawler cranes has led to the current high energy tamping levels first being performed on a regular basis in France in 1970 and subsequently in Britain 1973 and in North America in 1975 (Scolombe, 1993).

Although it's not a new technique in ground improvement, the design of dynamic improvement remains as an empirical approach, relying heavily on designers' experience and judgment (Chow et al., 1991). Currently, design of dynamic compaction is restricted largely to predicting the depth of improvement at an end state where little or no further improvement to the ground is possible. The most widely used relation for predicting the depth of improvement is based on the energy per blow (Menard and Broise, 1976; Lukas, 1992) and is expressed in the form below (Lee and Guu, 2004).

$$d_{max} = \lambda\sqrt{WH} \quad \text{.....} \quad (1.1)$$

Where d_{max} is the depth of improvement and λ is an empirical coefficient, which somewhat accounts for the soil type, dropping mechanism (true free fall or dropping with a lifting wire) and groundwater level, typically ranging from 0.3 to 0.7. Lucas (1986) and, Luango (1992) and others have discussed the factors influencing the effectiveness and improvement depth in dynamic compaction.

1.3.1 IMPACT ENERGY AS COMPACTIVE EFFORT

In dynamic compaction of soils, the impact of the tamper onto the ground generates three types of seismic waves that carry the energy. These waves, namely; Compression, Shear and Rayleigh waves have different attenuation and distribution characteristics. Rayleigh waves are also called the surface waves, since they travel along the surface of the

medium that they've been generated. On the other hand, shear and compression waves travel through the soil medium with different velocities and energy levels. When densification of the ground during dynamic compaction is taken into account, it can be supposed that the densification effect is only obtained by the energy distributed by compression waves. These waves travel through the ground on a spherical wave front as shown in figure 1.1 and the maximum energy exists on the vertical axis of symmetry reducing with increasing angle from the symmetry axis.

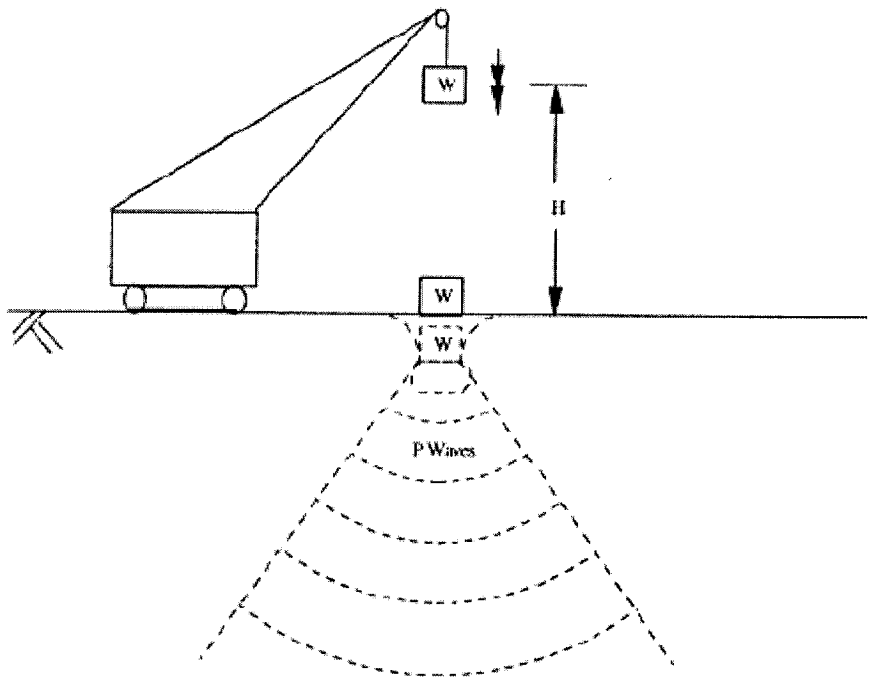

Figure 1.1: Schematic of Dynamic Compaction (Pan and Selby, 2002)

1.4 OBJECTIVE OF THE THESIS

The objective of this research is first to review the literature for the problem stated. Then it is intended to develop a theory to predict the level of compaction of a thin subgrade layer overlying a deep deposit. Accordingly, the role of the deep deposit, the impact energy applied and the thickness of the subgrade layer will be examined. Design theory and procedure will be given for practical purposes.

CHAPTER 2

LITERATURE REVIEW

2.1 GENERAL

In the literature, few reports can be found dealing with Dynamic Compaction. Even so, they're primarily focused on the amount of treatment achieved as obtained through experimental and field tests. Some reports were oriented in the development of a better understanding of the behavior of soil subjected to Dynamic Compaction.

The effect of a deep soft deposit underlain a thin subgrade layer to be compacted by Dynamic Compaction has received little attention in the field of Geotechnical Engineering. Nevertheless, the problem has been studied statically, in terms of Compaction and Foundation Settlement, but no effort were given to examine the effect of compacting the soil using dynamic loading.

2.2 FINITE ELEMENT ANALYSIS IN DYNAMIC COMPACTION

Pan and Selby (2002) simulated the dynamic compaction of loose soils under dynamic loads numerically, using ABAQUS© [Hibbit, Karlsson and Sorensen, Inc., 1998] to develop a full axisymmetric elasto-plastic finite element model of the soils. They simulated the impact of the dropping mass on ground surface in two ways:

1. A force-time input was imposed having the same characteristic shape of the deceleration of the mass after impact.

2. A rigid body impacting collision onto the surface was applied assuming free fall. They made comparisons of the ground waves, peak particle accelerations with depth, mass penetration (imprint, or crater depth) and peak particle velocity on the ground surface.

Pan and Selby have used the constitutive model of the classical Mohr-Coulomb failure criterion. It is an elasto-plastic model with a yield function of the Mohr-Coulomb form; which includes isotropic cohesion hardening/softening. The total stress approach was followed without reference to the pore water pressure, since the duration of each impact was measured in milliseconds.

As the first type of loading stated above, they used force-time load plot which is shown in figure 2.1. The duration of contact was taken as 0.05 second and they assumed a peak dynamic stress of 800 kPa applied onto a circular patch of 4m. in diameter.

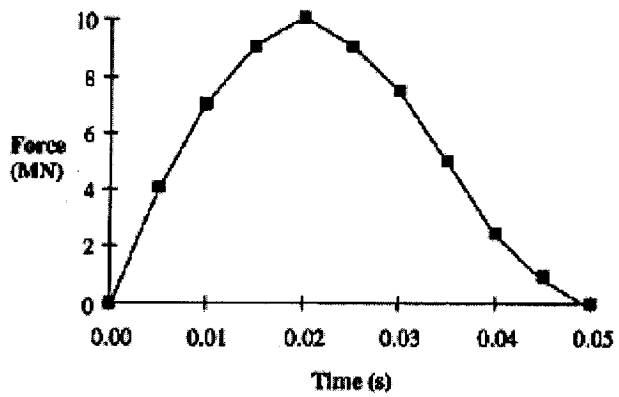

Figure 2.1: Force-time load plot (Pan and Selby, 2002)

For the impact collision, they imposed a rigid body impact load of a 10 Mg hammer dropping from 11.5 m, and striking the same surface patch of 4m diameter. The

input was initiated by a vertical velocity of 15 m/s, which was calculated as the velocity of the tamper when it hit the ground.

The development of the mass penetration (crater depth) was taken into consideration after the analysis. The maximum mass penetration was found to be 510 mm for the force-time load solution and 260 mm for the rigid body impact load analysis. For a single drop on the ground, the force-time load gave an overestimated depth of improvement as compared to the empirical estimation, whereas the rigid body impact load produced more reasonable results. It should be noted that the depth of improvement was categorized by the depth at which peak acceleration reached 2g; g being the acceleration of gravity.

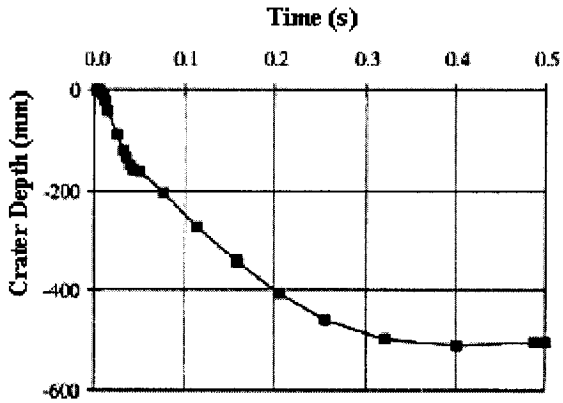

Figure 2.2: Crater depth for force-time load (Pan and Selby, 2002)

Subsequent to the evaluations above, they went on to study the effect of multiple drops and consideration was given to the cumulative effects of up to three drops on a single location. Upon their analysis, they found the depth of improvement nearer to

$2.0\sqrt{WH}$ than the more common range of 0.5 to $1.0\sqrt{WH}$. This variance was attributed to a possible overestimation of soil stiffness properties, an underestimation of the level of acceleration required to compact loose soils, and the restricting effect of saturated stiff soils at depth.

Lee and Gu (2004) proposed a new method for estimating the depth and degree of improvement in dynamic compaction. Their method was based on results from a number of finite element (FE) parametric analyses, which were, in turn, benchmarked by centrifuge model data. The FE parametric studies were conducted using in-house software CRISDYN (Goh et al. 1998; Gu and Lee 2002). The influence of soil properties, initial state, energy per blow, momentum per blow, and tamper radius on the depth and radius of improvement were investigated.

The impact of the tamper was modeled by considering the tamper as a stiff elastic block with an initial velocity calculated from the drop height, assuming free fall. A two dimensional axisymmetric FE mesh, shown in figure 2.3, was used to model the tamper and ground. The constitutive model used for this study was the cap model proposed by Dimaggio and Sandler (1971) for blast and dynamic loading on soils, with a nonlinear volumetric hardening law.

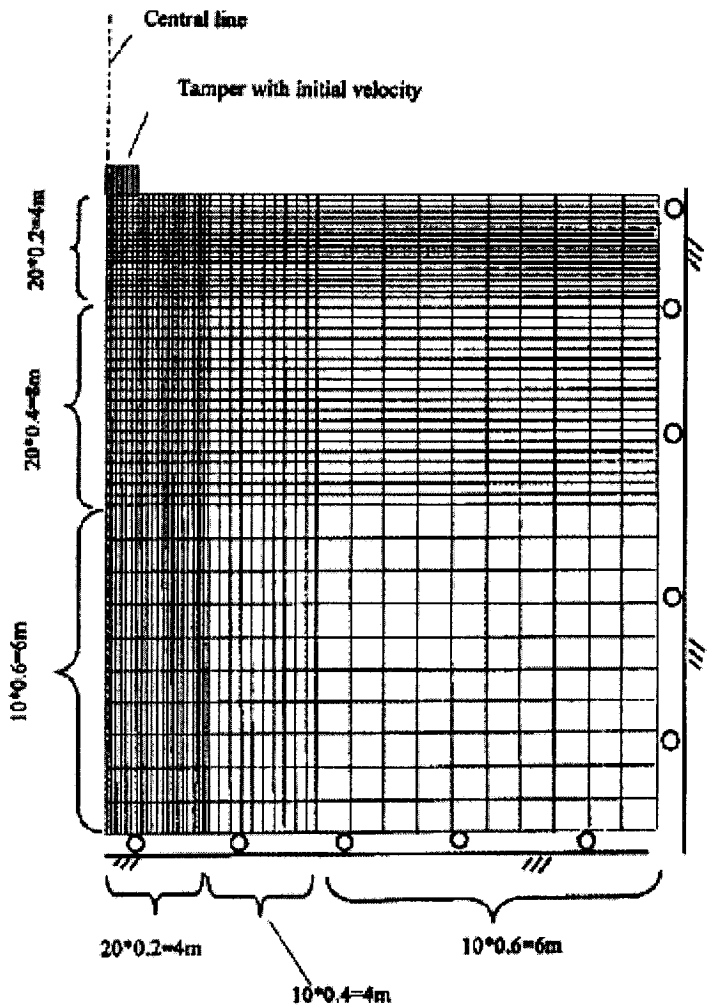

Figure 2.3: Two-dimensional finite element mesh (Lee and Gu, 2004)

To evaluate the effect of momentum and energy per blow on DC, they used 5 different weight and height combinations and obtained the computed increase in crater depth with successive impacts for all combinations. Over the range of energy and momentum per blow examined, they concluded that crater depth increased with momentum as well as energy per blow. The maximum achievable depth of improvement was found to be proportionally more with momentum than with energy per blow. They explained the influence of momentum per blow in terms of the increasing efficiency of

energy transfer with increasing momentum. For a given energy per blow, using a heavier tamper weight and lower drop height would result in a larger momentum of impact. For each combination, they also found an optimal tamper radius, which maximizes the depth of improvement.

2.3 PEAK DYNAMIC STRESS IN DYNAMIC COMPACTION

Wayne and Jones (1983) suggested an analytical solution to the peak dynamic stress occurred upon the impact of falling weights in dynamic compaction. As a simple approximation, they assumed the dynamic force-time response upon impact as a triangular impulse loading.

Using the conservation of momentum, the area under the force-time curve should equal the change in momentum:

$$\frac{1}{2}F_{max}\Delta t = m\Delta v \quad \text{..... (2.1)}$$

In which F_{max} = peak dynamic force $= ma_{max}$; Δt = total time for deceleration; m = mass of weight $= W/g$; Δv = change in velocity; a_{max} = peak deceleration; and g = gravitational constant = 32 ft/sec^2 = 9.8 m/sec^2.

For a free fall system, the velocity upon impact ($v_i = \sqrt{2gH}$) will equal zero after deceleration is complete so that:

$$F_{max} = \frac{2W\sqrt{2gH}}{g\Delta t} \quad \text{..... (2.2)}$$

Actually, friction in the system inhibits a true free-fall of the weight. Assuming the natural frequency (f_n) for the system to be:

$$f_n = \frac{1}{T} = \frac{1}{2}\sqrt{\frac{k}{m}} \quad \text{.....(2.3)}$$

In which $T = 2\Delta t$ = period of vibration; $k = 4Gr_o/(1-v)$ = vertical stiffness of the system; G = shear modulus; r_o = radius of the mass; and v = Poisson's ratio, then, equation (2.3) can be rewritten as:

$$\frac{1}{2\Delta t} = \frac{1}{2\pi}\sqrt{\frac{k}{m}}; \qquad \Delta t = \pi\sqrt{\frac{m}{k}}$$

$$\Delta t = \pi\sqrt{\frac{W/g}{\frac{4Gr_o}{1-v}}} = \pi\sqrt{\frac{W(1-v)}{4Gr_o g}} = \sqrt{\frac{\pi^2 W(1-v)}{4Gr_o g}}$$; then the dynamic force becomes:

$$F_{max} = \frac{2W\sqrt{2gh}}{g\sqrt{\frac{\pi^2 W(1-v)}{4Gr_o g}}} = \frac{\sqrt{4W^2 2gh}}{\sqrt{\frac{\pi^2 W g^2 (1-v)}{4Gr_o g}}} = \sqrt{\frac{32WHGr_o}{\pi^2(1-v)}}$$

Then the maximum dynamic stress at the point of impact becomes:

$$\sigma_{max} = \sqrt{\frac{32WHGr_o}{\pi^2(1-v)}} \cdot \frac{1}{A_p} \quad \text{..... (2.4)}$$

Where A_p = area of the pounder and G is the shear modulus of soil.

Reasonable predictions of peak dynamic vertical stress were made by this simple method when compared with measured stresses.

2.4 MATERIAL DAMPING

The amplitude of energy waves generated upon each impact on the ground is lost by two damping mechanisms. The loss in amplitude due to spreading out is called geometric damping. In addition to the above damping, there is another type of loss resulting from absorption in real earth material (Das, 1993).

The geometric damping is due to natural attenuation of the amplitude and is only dependent on site geometry. However, the case of material damping is a complex issue since it depends on many parameters, such as; strain level, confinement, cyclic shear strain amplitude and the ratio of high strain shear modulus to low strain shear modulus.

After an extensive survey of in-situ damping ratios of soils in various strain and loading conditions, Ishibashi and Zang (1993) concluded that damping ratio of soils is highly dependant on the ratio of G/G_{max} and they suggested the following formulation for estimating damping ratios for wide variety of soils.

$$D = \frac{0.333\left(1+e^{-0.0145 Ip^{1.3}}\right)}{2}\left[0.586\left(\frac{G}{G\max}\right)^2 - 1.547\left(\frac{G}{G\max}\right)+1\right] \quad \text{..... (2.5)}$$

where I_p is the plasticity index of soil.

It should be mentioned that the maximum damping ratio of sandy soils at high strain levels ($\gamma \geq 10^{-2}$) with Ip=0 is equal to 33%, which is also a representative value from previous researchers.

As shown by Hansbo (1978), the shear modulus relevant to the large strains developed during dynamic compaction is about one-tenth of the low amplitude shear modulus as determined from geophysical tests (G= $\rho V_s^2 / 10$ and V_s being the shear wave velocity). Accordingly, the in-situ damping ratio of soils during dynamic compaction may be approximated by incorporating this ratio in the damping ratio formulation above.

2.5 DISCUSSIONS

Based on the literature review presented herein, it can be noted that efforts were made by the researches to overcome uncertainties in solving dynamic compaction. Due to the extreme complexity of the problem governed by inter-related dynamic soil parameters and highly nonlinear behavior of the soil itself has prevented the researchers to simulate Dynamic Compaction with 100% accuracy. In that regard, a great deal of assumption and simplification has to be made to perceive the governing parameters of this sophisticated problem. With emerging computer technologies, especially in the analysis of soil subjected to dynamic loading, a better and efficient implementation of Finite Element method of analysis can be developed to simulate the case stated.

In the study of Pan and Selby, the force-time plot used to evaluate the impact of the falling weight does not account for the stiffness of the soil. Applying a force-time plot

taken from a site with unknown soil parameters on a soil with assumed parameters in a finite element code does not offer much accuracy regarding the dynamic soil behavior. Moreover, multiple drop analysis conducted on predicted soil parameters after each drop yields unrealistic results in terms of depth of improvement as stated by the authors. The effect of material damping is also not taken into account in studies presented in the literature review which somewhat ignores the amount of the energy to be absorbed by the material.

CHAPTER 3

NUMERICAL MODEL

3.1 GENERAL

In this study, numerical model of Dynamic Compaction in a two-layered soil medium is developed. The model is constituted by a Finite Element Programming named "Plaxis 8.2" which uses an add-on module.

3.2 NUMERICAL MODEL

In the study presented, an axisymmetric model with 4^{th} order 15-node triangular elements is used. The axisymmetric model is selected with reference to studies conducted in the literature and the condition of the problem itself, where a circular tamper is dropped onto the ground. It is evident that an axisymmetric model is suitable for circular structure with a uniform radial cross section and loading scheme around the central axis. The deformation and stress state are assumed to be identical in any radial direction. The x-coordinate represents the radius whereas the y-coordinate is the axial line of symmetry.

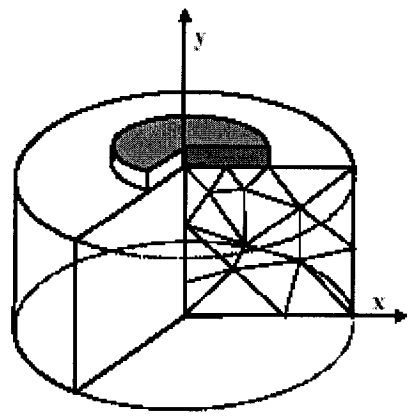

Figure 3.1: Schematic of an axisymmetric problem (Plaxis 8.2 Reference Manual)

3.3 PROBLEM GEOMETRY AND BOUNDARY CONDITIONS

The geometry of the problem is defined as a thin subgrade layer overlying deep deposit. In this study, both the subgrade and the deposit are assumed to be sand with various values of stiffness. The underlying layer was assumed to be 25m in depth and width, where the depth of the subgrade layer was vary in the range of 0.15m to infinity and covers the entire area of the deposit. The geometry of the problem is selected as stated above to eliminate confinement of the subgrade against the boundary conditions of the proctor mold.

The outer boundaries of the soil medium are supported by horizontal fixities at the vertical geometry lines and full fixities at the horizontal geometry line as shown in figure 3.2. However, in order to avoid the reflection of seismic waves generated upon impact, dynamic absorbent boundaries are placed on the bottom and on the right fixities. These boundaries ensure that an increase in stress in boundary is absorbed without rebounding. Trial calculations were performed using boundary elements at the interface between the two layers, the results showed no effects on the results obtained, and accordingly the analysis was performed having only the boundaries at the extreme planes making the horizontal and the vertical geometry of the mesh.

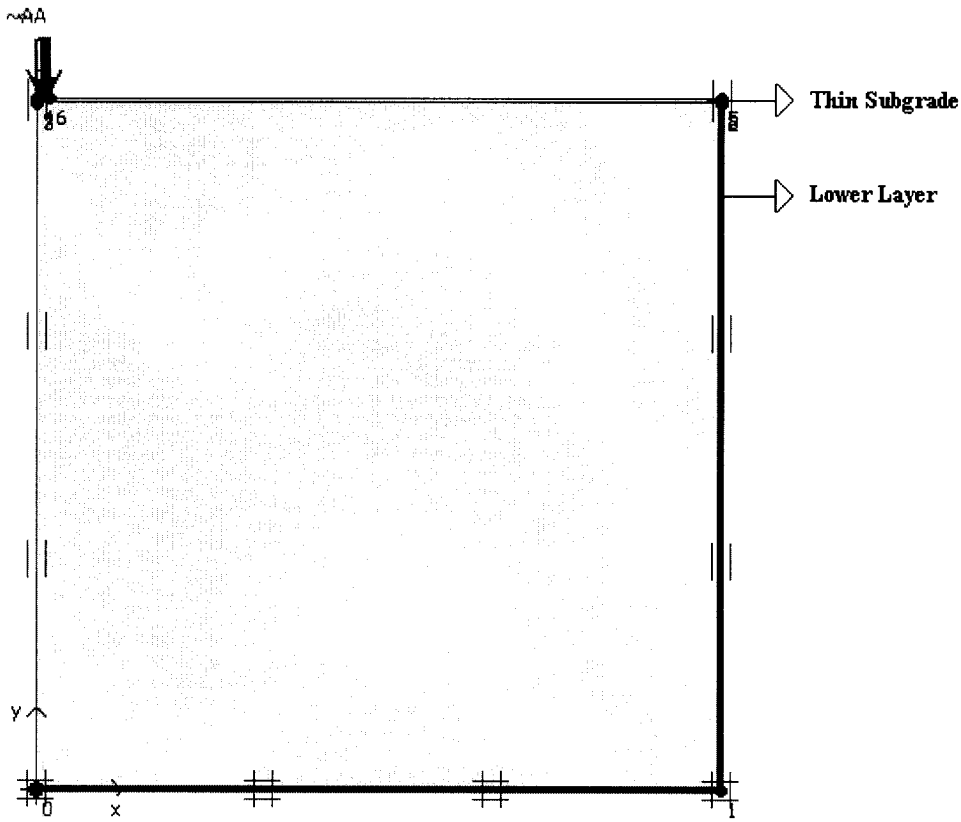

Figure 3.2: Problem Geometry and Boundary Conditions

Since the application of impact energy and the associated deformations in soil are concentrated at the point of impact and in the vicinity of the subgrade layer, mesh refinements are indispensably required in these zones. Trial tests were performed to establish the level of mesh fineness on the results obtained. The final mesh is shown in figure 3.3.

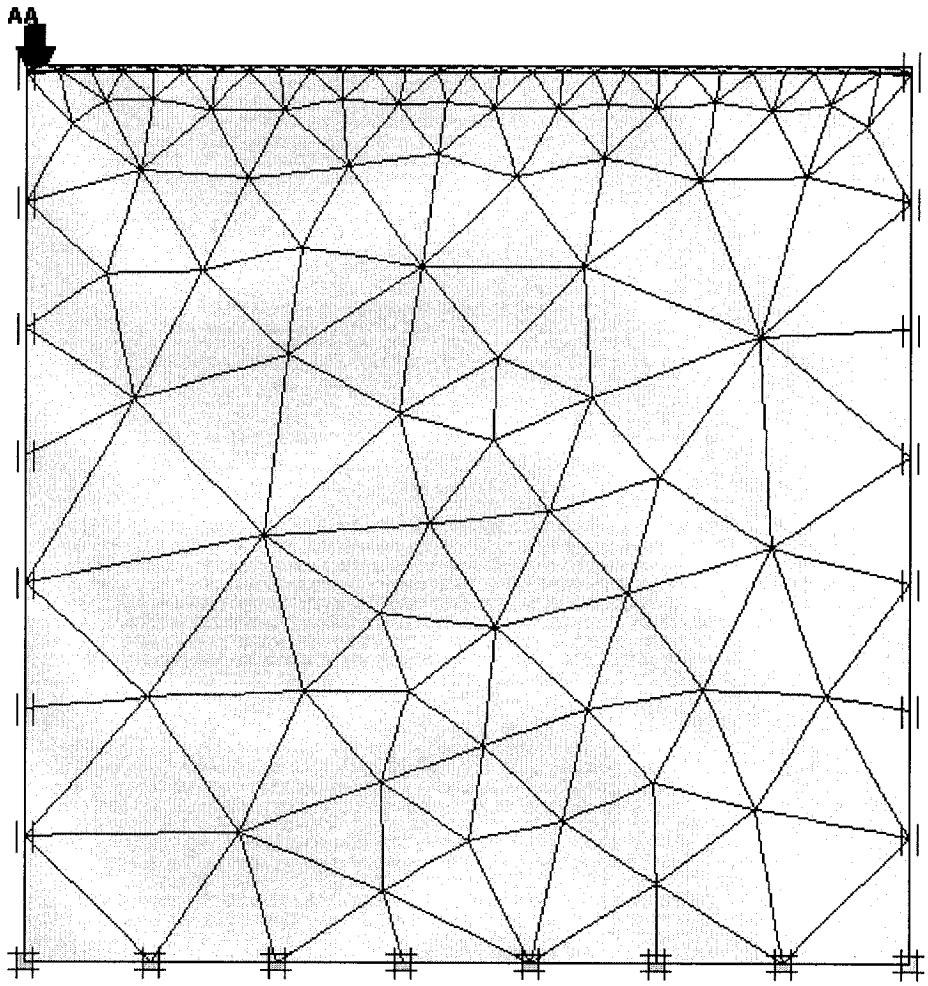

Figure 3.3: Generated Mesh

Due to the nature of the "dynamic" problem, the mechanical properties of the soil and deformation characteristics will change continuously during testing. Accordingly, the subgrade layer is modeled by using the "Hardening Soil Model". After each step of calculations, the stiffness matrix of the soil is updated; this was used for the calculation of the next step.

On the other hand, since the underlying layer is much deeper and will obviously exhibit less deformation than the upper layer, it is modeled by using the Mohr-Coulomb

Model (Perfect Plasticity). This model has a fixed yield surface, i.e. a yield surface that is fully defined by model parameters and not affected by plastic straining.

3.4 DYNAMIC LOADING

The dynamic loading during each drop of the compaction process is defined as a transient load, which is in the shape of a half-sine wave. The load starts from zero and reaches the peak value beyond which the load starts to drop. This uniform load is applied on the base area of the tamper, which is taken in this study as the base area of a patch 1m in diameter. Peak dynamic stresses for each energy level are calculated based on equation (2.4), whereas energy levels to obtain the desired densification in the subgrade are calculated using equation (1.1).

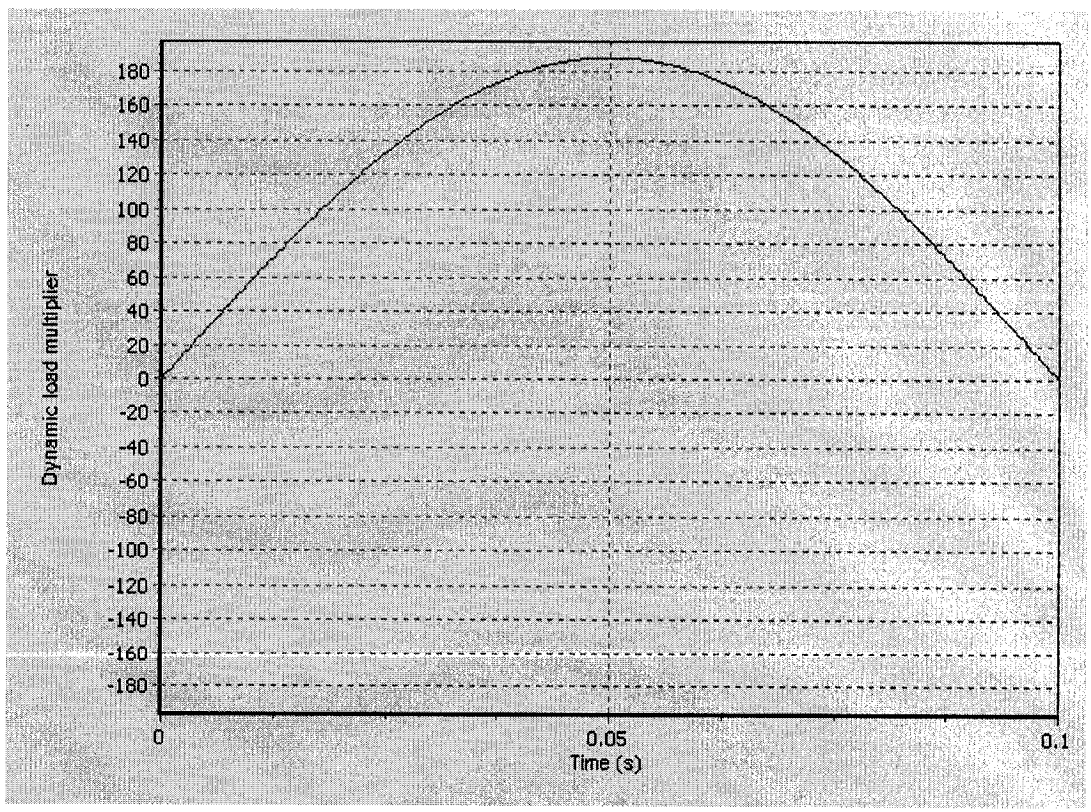

Figure 3.4: Transient Load due to Impact

The duration of the contact for each impulse loading is assumed to be 0.1 second, which corresponds to a transient harmonic load of 5 Hz in frequency having amplitude that equals the peak dynamic stress formed upon each impact. This duration of loading is quite reasonable given the fact that the associated vibrations in dynamic compaction are in the range of 2 to 10 Hz in most of the cases. However, the duration of impact unfortunately changes as the soil is being improved but since there is no rational means of evaluating this change for the duration of each impact, it will be neglected in this study. Moreover, the peak dynamic stress also changes as the soil is being improved due to the change in its stiffness. Nevertheless, the evaluation of the change in peak stress due to increase in stiffness and incorporation of this change to the finite element programming is not possible. In that regard, the change in the peak dynamic force has to be neglected.

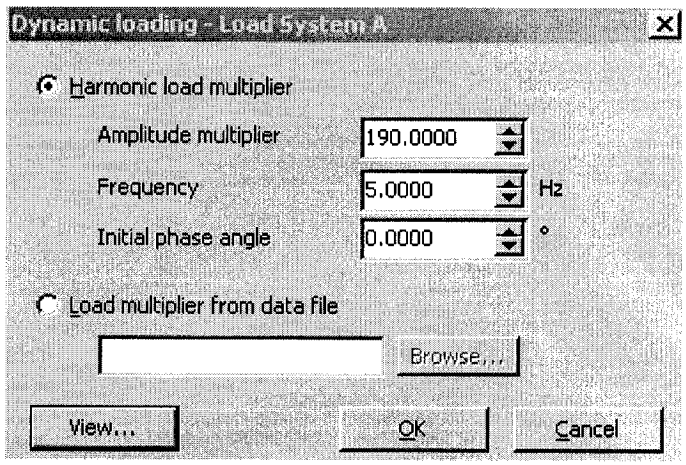

Figure 3.5: Harmonic Load Multipliers

Figure 3.5 shows the input values of the dynamic load system, named as Load System A. The amplitude multiplier is the actual amplitude value of the dynamic load which corresponds to the peak dynamic stress in KN/m^2. Frequency values are entered in

Hertz and produce a transient loading with the shape of a half-sine wave when the initial phase angel is entered as zero. The produced transient loading (i.e., a single impact) is shown in figure 3.4.

The duration of the unloading period (i.e., the time period between each impact) has been taken in a way that this time period will allow the dynamic stress to be distributed within the soil mass and all the rebound effect at the point of impact and the interface take place. After a number or loading-unloading tests in the model presented, it is found that twice the impact duration is sufficient to be taken as the duration of unloading; after which soil is ready to be applied the successive impact.

3.5 SOIL TYPES

In order to evaluate the effect of the stiffness of the deposit, the sand making the deposit material was tested within the range of very loose to very dense states. The subgrade is taken as loose sand layer with different values in depth.

In order to study the effect of the level of energy per drop on the level of compaction achieved, tests were conducted using 6 drops with 5 different energy levels impacted on the ground surface.

Since it is required to enter the Oedometer Modulus (M) for the upper layer in the hardening-soil model, this value is calculated using the relation between the Elasticity Modulus and the Oedometer Modulus of soil as given by the formula;

$$M = \frac{E(1-\upsilon)}{(1-2\upsilon)(1+\upsilon)} \quad \text{..... (3.1)}$$

Where: E and υ are the elasticity modulus and Poisson's ratio of the sand material, respectively.

In order to calculate the Damping Ratios of the sand; Rayleigh α and Rayleigh β for all stiffness levels of the soils used in the analyses, the ratio of dynamic shear modulus to maximum shear modulus were taken into account. Due to the fact that during dynamic compaction of soils low frequency vibrations and higher deformation and strain values will be produced, the dynamic shear modulus of soil is taken as one-tenth of its initial value. Therefore, the G/G_{max} value for each stiffness levels of the lower layer will be taken as approximate values; regarding how much the underlying layer would be affected from dynamic loading. In that regard, the G/G_{max} value has to increase as the stiffness of the lower layer is increased and reach 1 for the stiffest case where the lower layer is expected to exhibit no deformation due to the impact on its overlying layer. The values of the ratio of shear moduli and other parameters to be incorporated in the analyses are shown in table 3.1. It should be noted that, these soil parameters represent a subgrade layer of fixed stiffness and 6 types of lower layers, from very loose sand to dense sand. Values of soil parameters are taken as average values for loose, normal, and dense sand were taken from Das (1996).

Table 3.1: Soil Parameters used with the numerical model

Soil Type	γ_{unsat} (kN/m^3)	γ_{sat} (kN/m^3)	$k_x=k_y$ (m/sec)	E (kN/m^2)	M (kN/m^2)	C (kN/m^2)	Φ (°)	ν	G/Gmax	α	β
Upper layer	17.5	19.0	0.00005	10000	11111	0.2	30	0.3	0.1	11.87	0.006
Lower layer 1	13.5	15.0	0.00005	2500	-	0.2	25	0.2	0.1	11.87	0.006
Lower layer 2	15.5	17.0	0.00005	5000	-	0.2	27	0.2	0.3	8.22	0.00416
Lower layer 3	19.0	20.0	0.00005	15000	-	0.2	32	0.35	0.5	5.199	0.00263
Lower layer 4	19.5	20.5	0.00005	20000	-	0.2	35	0.35	0.7	2.85	0.00144
Lower Layer 5	19.5	20.5	0.00005	30000	-	0.2	40	0.4	0.8	1.929	0.00098
Lower Layer 6	20.0	21.0	0.00005	40000	-	0.2	45	0.45	1.0	0.545	0.00028

3.6 MATERIAL DAMPING RATIOS

In finite element programming used in this study, Rayleigh damping is utilized as an input for material damping, which lumps the damping effect within the mass and stiffness matrices of the system. Rayleigh alpha is the parameter, which determines the influence of the mass in the system, whereas Rayleigh beta is the one reflecting the influence of stiffness.

$$[C] = \alpha[M] + \beta[K] \quad \text{..... (3.2)}$$

These two damping coefficients can be determined from two given damping ratios that correspond to two frequencies of vibration. However, in this study, due to extreme dependence of damping ratio on dynamic shear modulus of soils, damping ratio will be taken as a variable governed by the in-situ dynamic shear modulus, rather than the frequency level. Accordingly, G/G_{max} value in formula (2.5) will be taken as 0.1 to 1.0 to calculate damping ratios of subgrade and the underlying layer depending on expected deformation levels to be experienced by the soil during compaction. In order to quantify alpha and beta parameters with formula (3.3) below, same damping ratio for the corresponding soil type will be used for frequency levels of 5 and 10 Hz, which are found to be common levels of vibration in impact compaction of soils.

$$D = \frac{\alpha}{2\varpi} + \frac{\beta\varpi}{2} \quad \text{..... (3.3)}$$

3.7 ENERGY LEVELS AND NUMBER OF TESTS

Note that the peak dynamic stress is calculated with respect to the stiffness and target depth of the subgrade (0.15m) since it is the layer to be compacted. Calculated energy

levels upon each impact of a tamper 1m in diameter and the peak dynamic stresses are presented in table 3.2 below.

Table 3.2: Energy Levels and Peak Dynamic Stresses for Different Depths of Sand Layer

Depth of Subgrade Layer (m)	Energy Level for target depth	Energy per Drop (Nm)	Peak Dynamic Stress (KN/m^2)
0.15 to Infinity	EL_1 (λ=0.3)	2500	190.00
	EL_2 (λ=0.4)	1406.25	142.5
	EL_3 (λ=0.5)	900	114.0
	EL_4 (λ=0.6)	625	95.0
	EL_5 (λ=0.7)	459.24	81.5

Table 3.3: Number of Tests

Depth of Subgrade	Underlying layer stiffness	Energy Level	Number of Tests
0.15 m	6 stiffness levels	5 Energy Levels	30
0.30m	6 stiffness levels	5 Energy Levels	30
0.45m	6 stiffness levels	5 Energy Levels	30
0.60m	6 stiffness levels	5 Energy Levels	30
0.75m	6 stiffness levels	5 Energy Levels	30
Infinite	-	5 Energy Levels	5

3.8 MODEL VALIDATION

The validation process of the numerical model was performed using experimental and numerical studies available in the literature. For this purpose, the data from an extensive experimental study of Poran et al. (1992) and Poran and Rodriguez (1992) will be utilized for comparison with the results of the present model.

For validation of the numerical model presented in this thesis, tamper settlement data from the experimental and numerical studies will be of interest; therefore data from these studies will be used.

3.8.1 SOIL TESTED

The soil used for the experimental study was dry Boston sand with particle diameters ranging between 0.09 mm and 0.9 mm, with D_{10}= 0.28 mm, and D_{60}= 0.73 mm. The sand was classified as SP according to the ASTM D2487 (USCS). Other properties were tested in accordance to their respective ASTM standards and the results are summarized in the following table below.

Table 3.4: General soil properties used in experiments (Poran et al., 1992)

Parameter	Value
Unit weight (kN/m^3)	15.5
e (void ratio)	0.74
Specific Gravity	2.674
Φ	34.2°

3.8.2 EXPERIMENTAL TEST PROCEDURE

The test layout consisted of a 1.22 × 1.22 × 1.22 m cubic steel tank filled with sand. The tampers used in core tests were steel plates in two diameters: 15.2, and 10.2 cm, which were set up in various specified tamper weights. The tamper was lifted with an electromagnetic mount for quick release and free fall to be carried out to 18 drops. Special attention was given to tamper dimensions, weights, and drop heights in order to minimize boundary and model scaling effects. The details of the testing program are shown in the table 3.5 below.

Table 3.5: Energy levels and tamper diameters for the experimental test program

Tamper weight (N)	Tamper diameter (cm)	Drop height (m)	Energy per drop (Nm)
220	10.2	2.0	440
220	10.2	1.0	220
220	15.2	2.0	440
332	15.2	0.67	220
332	15.2	1.99	660

3.8.3 VALIDATION

With the available soil data given by the authors, soil parameters shown in table 3.6 were incorporated into the numerical model using some basic correlations and interrelations between the given soil parameters and parameters to be used in the numerical model.

Table 3.6: Soil parameters to be used in numerical model

Parameter	Value
E (kN/m^2)	15000
ν (poisson's ratio)	0.3
$\gamma_{unsaturated}$, $\gamma_{saturated}$ (kN/m^3)	15.5, 19.8
Φ	34°
Rayleigh α, β	11.87, 0.006

Peak dynamic stresses upon each impact are calculated with formula 2.4, results of which can be seen in table 3.7. Settlement values at the point of impact up to 12 drops are taken as outputs from the numerical model.

Table 3.7: Calculated peak dynamic stresses for experiments

Tamper weight (N)	Tamper diameter (cm)	Drop height (m)	Peak Dynamic Stresses (kN/m^2)
220	10.2	2.0	2997.329
220	10.2	1.0	2114.447
220	15.2	2.0	1647.664
332	15.2	0.67	1162.318
332	15.2	1.99	2018.350

The average of settlement values from the tests summarized in table 3.5 are compared with the actual experimental and numerical results as shown in figure 3.6 below.

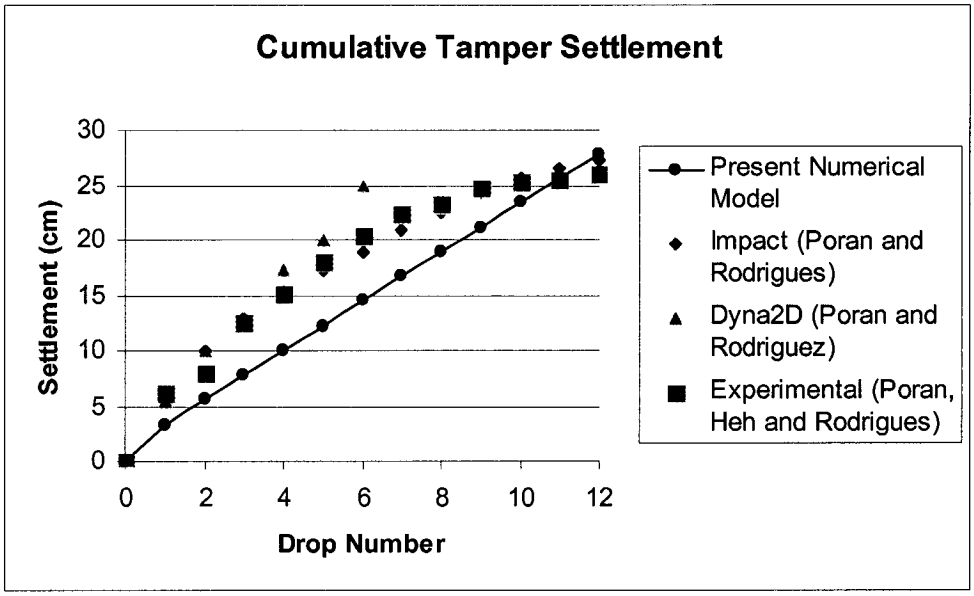

Figure 3.6: Comparison of deformation values after each impact

It can be seen from the figure that, vertical deformations at the point of impact show good agreement; validating the analytical approach to evaluate the peak dynamic stress upon impact and the duration of loading and unloading phases. However, since the numerical model is consisted of absorbent boundaries to eliminate confinement in the soil medium, when highly localized dynamic stress is applied onto the soil in a tank of relatively small dimensions, the lower boundary of the problem model (the base of the tank in the experimental study) exhibits downward deformation and causes deformation at the point of impact, thus eliminating the hardening effect. It can be concluded that, the numerical model and method of analysis provide a good inside to the deformation values up to a drop number of 12, after which soil in the tank is expected to show the hardening effect in this test. This downfall of the model will not be pronounced when the boundaries of the problem are infinitely apart from each other, allowing full energy distribution within the soil medium before the energy waves reach the absorbent boundary.

The maximum vertical deformation has occurred at the point of impact, as would be expected. Figure 3.7 and 3.8 show the deformed mesh and shadings of vertical deformation values upon impact, respectively.

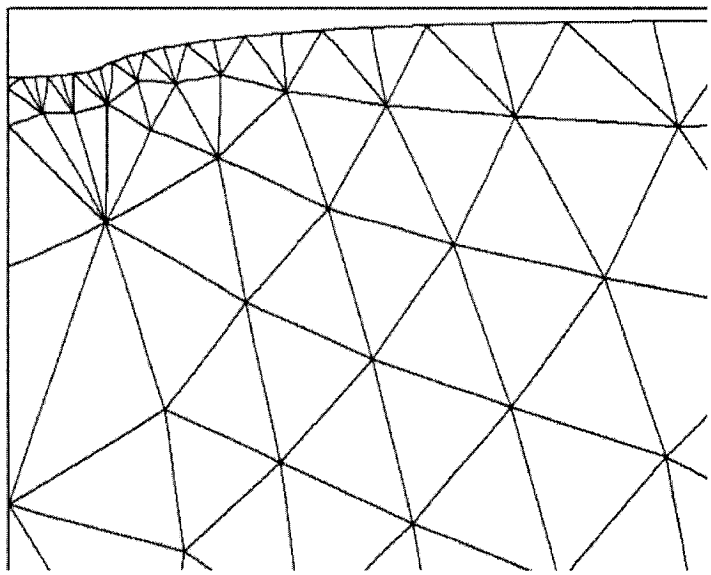

Figure 3.7: Deformed mesh upon impact

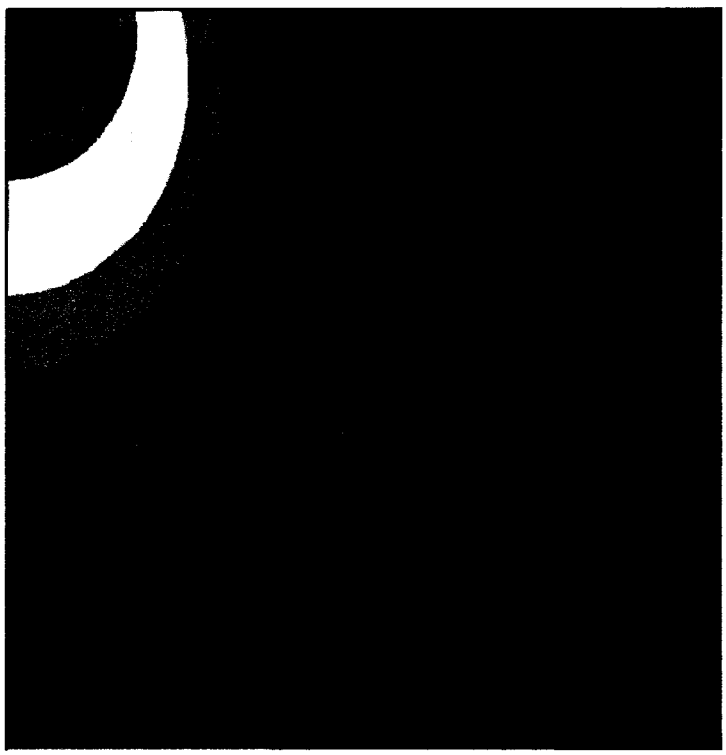

Figure 3.8: Shadings of vertical deformation upon impact

CHAPTER 4

TEST RESULTS

4.1 SIMPLIFIED PROBLEM MODEL

In this chapter, results obtained from the present numerical model will be presented. For this purpose, some assumptions will be made in order to maintain a comprehensive, yet simple approach to the nature of the problem.

Since the problem is the compaction achieved in a thin subgrade overlying a weak deposit, the compaction effort and stiffness levels of the both layers will be the governing parameters. In that regard, compaction effort consumed in the lower layer and the upper layer will be compared for various stiffness levels of the lower layer. For the sake of simplicity, each layer will be given dynamic stiffness constants (k) and taken as springs. When the compaction energy is applied on the two-spring system, each spring (soil layer) will take its share from this energy. To calculate the energy taken by each layer, vertical deformation values will be taken from the outputs of the numerical model for the point of impact and the interface between the layers. When the subgrade depth is increased from the target layer of compaction (15 cm in this study) to a higher value, as if a new subgrade layer is placed on the top of the first layer, the deformation at the interface of the first and the next layer will also be taken into consideration.

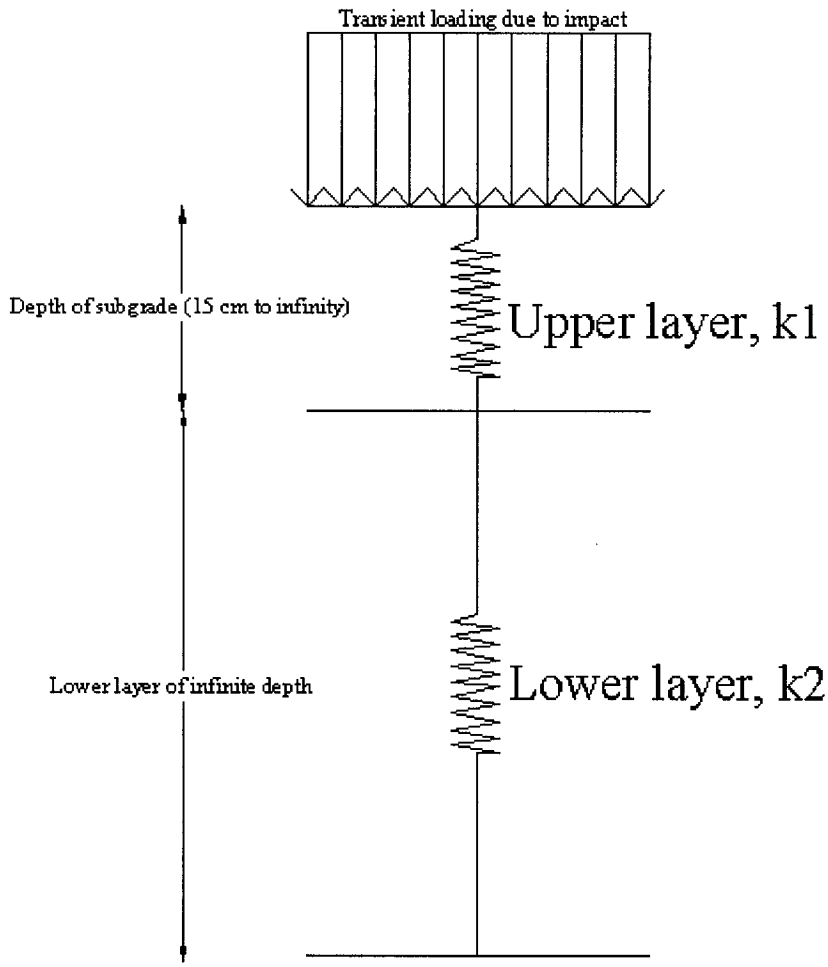

Figure 4.1: Schematic of the simplified problem model

4.2 ASSUMPTIONS REGARDING THE NUMERICAL APPROACH

Following assumptions are made before the results are taken:

i. When the soil is subjected to compaction energy at a pre-defined extent, no matter what type of material or soil is underlying it, it is going to absorb or filter the same amount of energy. The rest of the energy will be transferred to the lower layer material.

ii. The energy absorbed by the target depth of compaction of the upper layer will be taken from the condition that no boundary conditions exist in the soil medium; where the subgrade is to an infinite depth. This assumption will prevent the energy wave reflections due to an existing boundary.

iii. When energy waves reach the interface between the two layers, some energy will be absorbed and some will be reflected back to the upper layer depending on the resistance of the lower layer to this energy transfer. The highest level of compaction will be achieved when all the energy is reflected back to the upper layer. Accordingly, infinitely small compaction will be pronounced when the energy transmitted to the lower layer is completely absorbed with minimum resistance. These two extreme conditions are the upper and lower boundary conditions of the problem.

iv. The compaction achieved in the upper layer (subgrade) will be a function of energy that is lost to the lower layer. The lower the energy lost, the higher the achieved compaction. The energies calculated will be equivalent spring energies and representative values for sake of comparison only; they do not reflect the exact amount of energy that has been used in the compaction process.

The table below shows the calculated dynamic stiffness constants for all layers used in analysis. The energy taken by each layer will simply be calculated as an equivalent spring energy given by the formula;

$$E = \frac{1}{2}kx^2 \quad \text{..... (4.1)}$$

Where; k is the stiffness and x is the vertical deformation of the spring.

Table 4.1: Calculated dynamic stiffness constants (k) for the upper and lower layers

Soil	G (kN/m^2)	M	r_o (m)	k (kN/m)
Upper layer	3846.154	0.3	0.5	10989.011
Lower layer 1	1041.667	0.2	0.5	2604.167
Lower layer 2	2083.333	0.2	0.5	5208.333
Lower layer 3	5555.556	0.35	0.5	17094.017
Lower layer 4	7407.407	0.35	0.5	22792.023
Lower layer 5	10714.286	0.4	0.5	35714.286
Lower layer 6	13793.103	0.45	0.5	50156.740

4.3 ONE DIRECTIONAL ENERGY FLOW APPROACH

It was already mentioned that the two-layer system is simplified by two springs attached to one another as shown in figure 4.1. In order to evaluate the mechanism and the rate of energy loss to the lower layer, a one-directional energy flow approach will be used as explained below.

When the compaction energy is applied on the ground surface, the energy will travel through the upper subgrade layer and be absorbed by this layer for the compaction to be achieved. The residual energy will be resisted by the lower layer to some extent and

the rest of the energy will be absorbed by the lower layer causing the loss in compaction energy. In that regard, the general formula of the percentage of energy loss can be written as follows, where EN_1 and EN_2 are the energies absorbed by the subgrade and the lower layer respectively.

$$\text{Compaction Energy Loss (\%)} = \frac{EN_2}{EN_1 + EN_{RESISTED} + EN_2} \times 100 \quad \text{..... (4.2)}$$

For one directional energy flow, it is straightforward to evaluate the energies absorbed by two layers for all depths of the subgrade. However, the resisted energy at the interface between two layers is hard to evaluate. On the other hand, it is obvious that the resisted energy by the lower layer would be a function of the absorbed energy by that layer; the lower the resistance the higher the energy absorbed by lower layer and vice versa. Moreover, for the upper and lower boundary conditions of the problem, the energy resisted will have no effect on the percentage of the compaction energy loss mathematically, as explained below:

With respect to formula 4.2;

For the lower boundary condition; when all the transmitted energy to the lower layer is absorbed, $EN_{RESISTED}$ will be zero and be omitted in the equation.

For the upper boundary condition, when all the transmitted energy to the lower layer is resisted, EN_2 will be zero and $EN_{RESISTED}$ will have no effect in the result.

In conclusion, the above mentioned one-directional energy flow approach will be employed for the evaluation of energy loss in a dynamic compaction process applied on a two-layer system. The resistance energy at the interface will not be included in the calculations due to its nature of being an internal mechanism that cannot be evaluated. This drawback of the approach is yet compensated by the fact that this internal mechanism is included in the problem as a function of the energy absorbed by the lower layer material which can be easily evaluated.

4.4 EVALUATION OF ENERGY ABSORBED BY THE SUBGRADE

As it was mentioned before, the energy to be consumed in the upper layer before the energy transfer at the interface will be the same, regardless of the stiffness of the lower layer. The table below shows the energy taken by the upper layer as energy waves move through and just about to reach the lower layer. These will be key values as to how much compaction energy will be shared by the two layers. Then the percentage of energy lost to the lower layer will be the ratio of energy taken by the lower layer to the total energy taken by the two layers.

Table 4.2: Deformation and energy values for homogenous subgrade after 6 drops

Energy Level	Deformation at the point of impact (m)	Deformation at interface of the target depth (m)	Energy taken by the target depth (Nm)	Energy lost below the target depth (Nm)	Loss in compaction (%)
EL_1	-0.0553	-0.0276	12600.19	4193.38	25.0
EL_2	-0.0399	-0.0192	6709.94	2035.00	23.3
EL_3	-0.0309	-0.0144	4099.97	1136.97	21.7
EL_4	-0.0251	-0.0114	2740.01	709.56	20.6
EL_5	-0.0210	-0.0093	1949.99	474.17	19.6
					Av: 22.0

As it can be seen on table 4.2, in the case of homogenous subgrade to an infinite depth, 20 to 25 percent of the compaction energy is lost below the target depth of compaction. The loss of energy is slightly lower in small energy levels (EL_4 and EL_5) than the one for high energy levels (EL_1 and EL_2). When compared with the "imaginary" site conditions in the proctor test, even though the subgrade is not underlain by weak deposit, an average of 22 percent of compaction effort is lost, due to the lack of confinement within the soil medium.

4.5 ENERGY TRANSFER FOR DIFFERENT DEPTHS OF THE SUBGRADE

It should be remembered that, in case of the target depth of compaction being equal to the depth of subgrade in hand, the only interface that the energy sharing between the two layers will be done through element-a as shown in the figure 4.2. On the other hand, when depth of the subgrade is increased from its initial value, there will be two elements to be taken into consideration. In this case, some energy will be absorbed by the lower layer through element-b and some energy will be lost below the target depth of compaction within the subgrade through element-a. The subgrade will actually "sense" the presence of a weak lower layer up to a certain depth before it behaves as a homogenous material. This case is represented by figure 4.3.

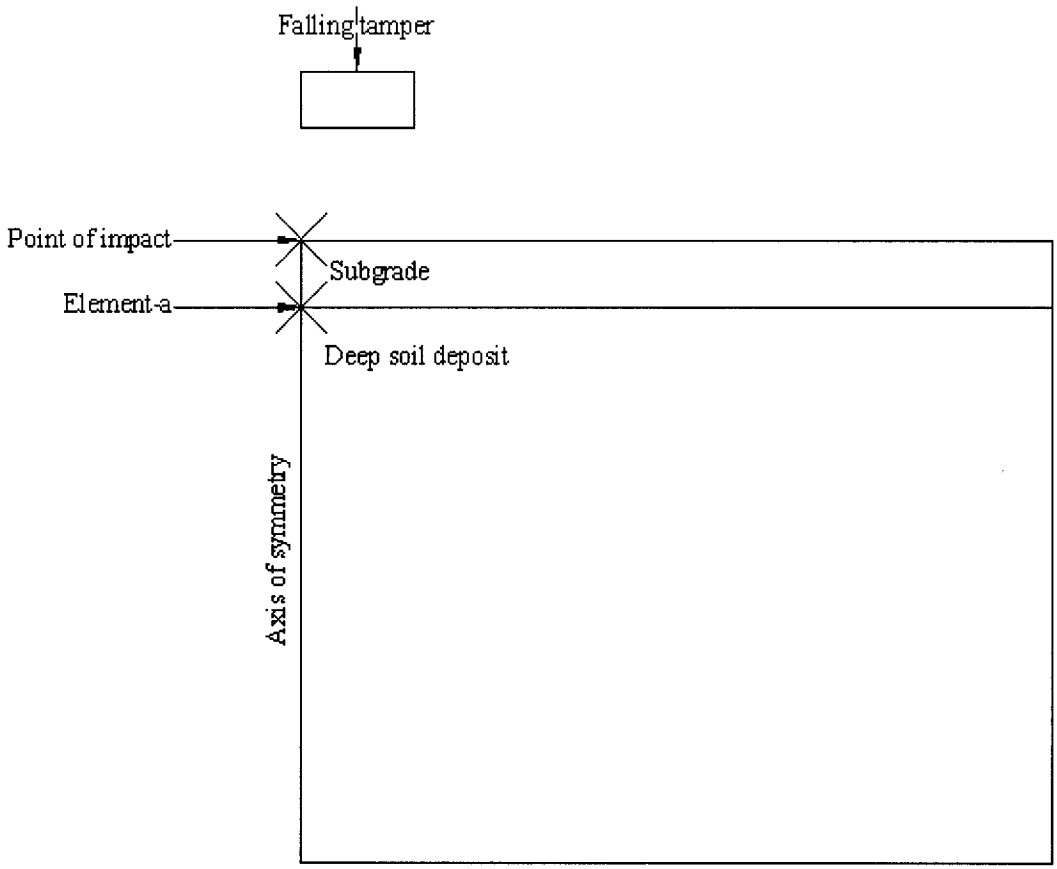

Figure 4.2: Point of impact and the interface; for subgrade depth = target depth

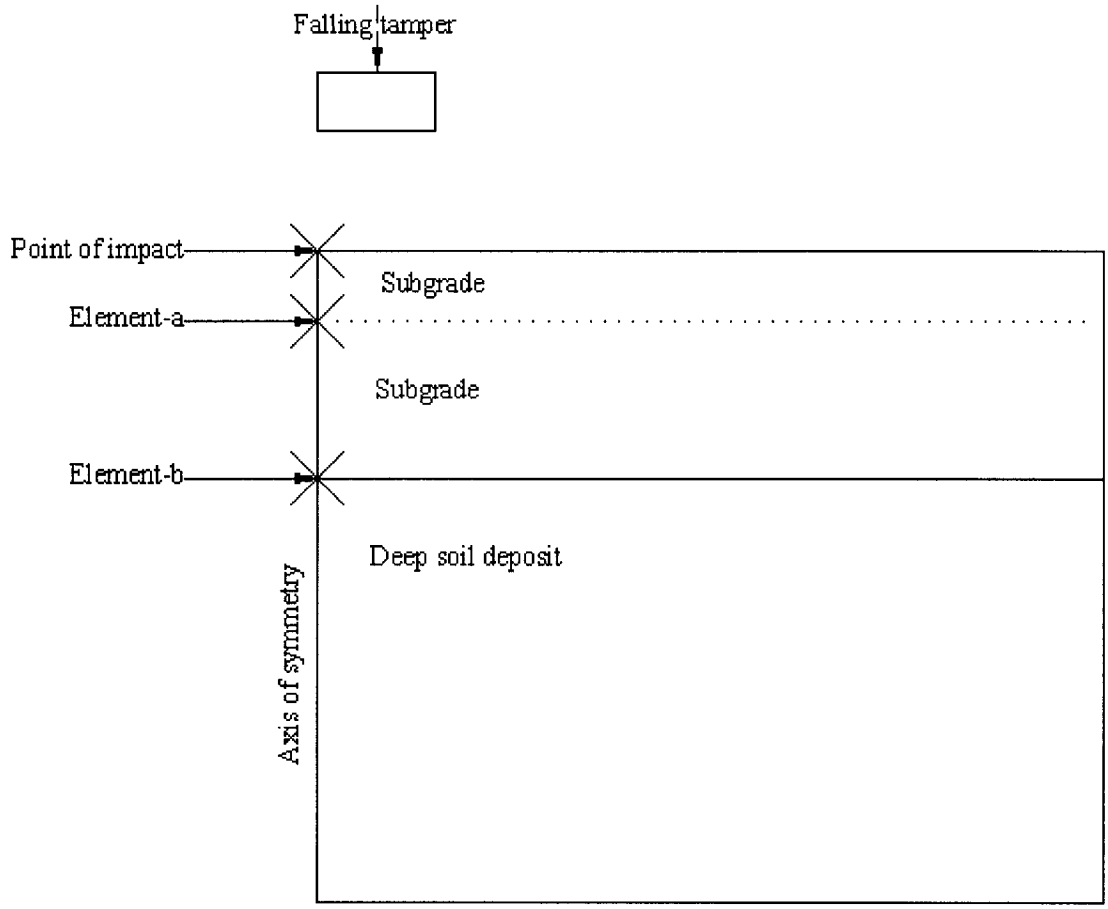

Figure 4.3: Point of impact and the interface; for subgrade depth > target depth

4.6 DEFORMED MESH UPON IMPACT

When the impact is applied onto the ground, soil particles will deform in all 3 dimensions; x, y, and z contributing to the vertical deformation of soil particles. However, since the numerical model in hand is an axisymmetric one with two degrees of freedom, only the horizontal deformation is contributing to the vertical movement. The deformed mesh upon impact for the homogenous case is shown in the figure 4.4. It can be noticed that there is a heave formation close to the perimeter of the tamper being less than the vertical deformation at the point of impact. This is the case encountered in the field

and is a characteristic of behavior of soil upon impact. It should be noted that, due to scale effect, the deformation of the mesh may be seem rather exaggerated.

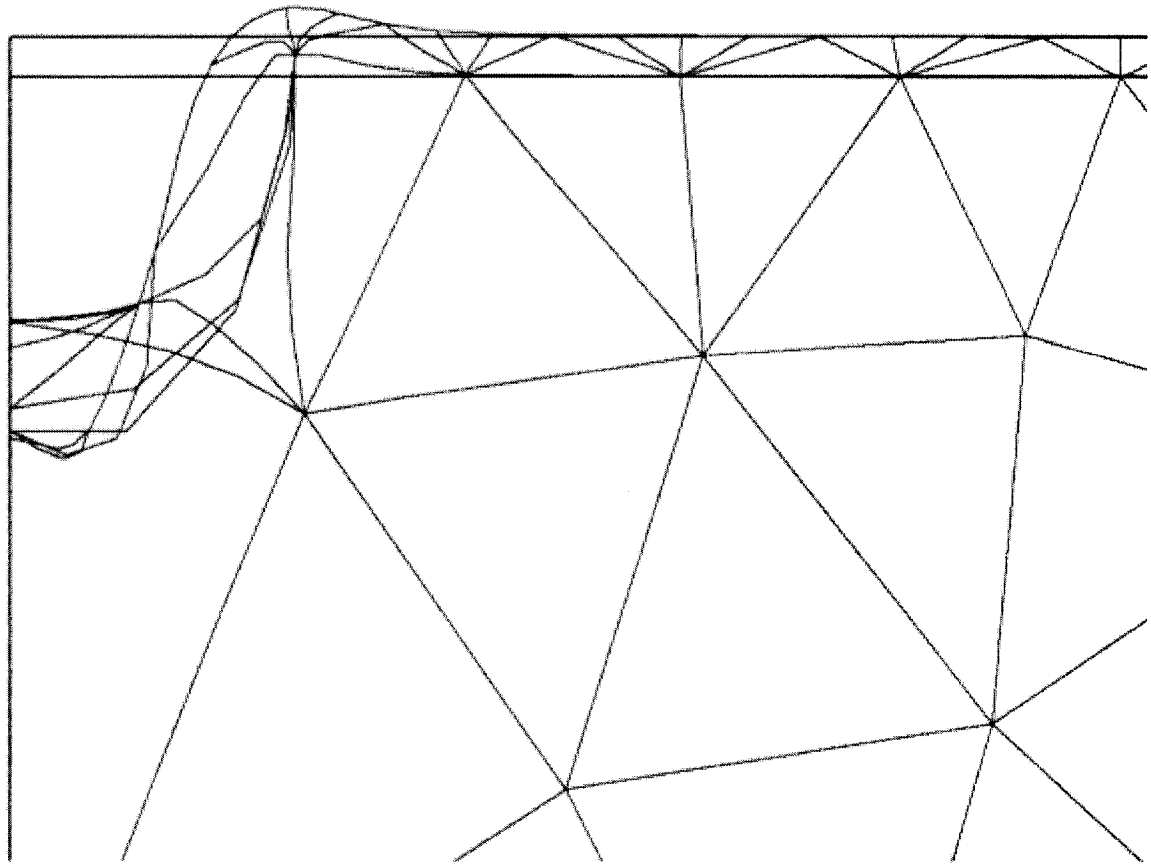

Figure 4.4: Deformed mesh upon impact (scaled to fit)

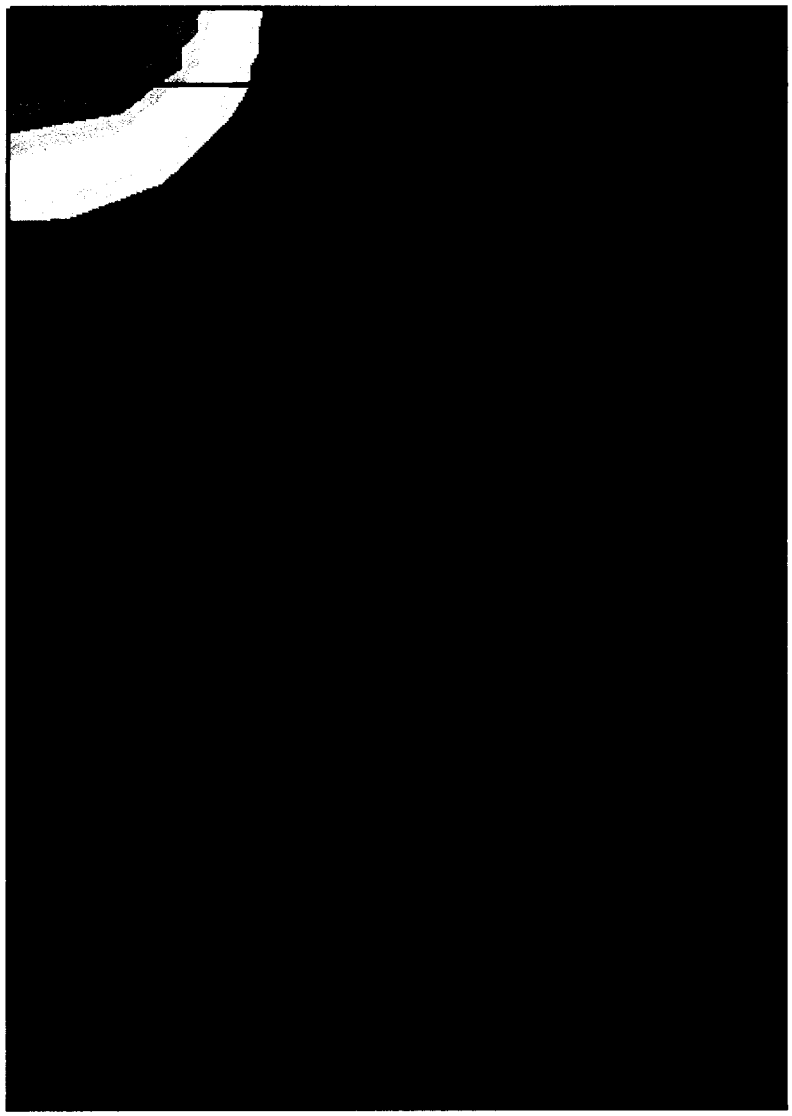

Figure 4.5: Shadings of vertical deformation upon impact

Figure 4.5 shows the zone of soil where most vertical deformation occurs after impact. The extent of deformation is the highest at the point of impact and is decreasing by depth.

4.7 RESULTS OF ANALYSES

Table 4.3: Deformation and energy values for 0.15 m subgrade (target depth=subgrade depth)

Lower layer stiffness	Energy Level	Deformation at element-a (m)	Energy Taken by the upper layer (Nm)	Energy lost to the lower layer (Nm)	Loss in Compaction (%)
E=2500 kN/m^2	EL_1	-0.2673	12600.19	93066.97	88.1
	EL_2	-0.1646	6709.94	35264.15	84.0
	EL_3	-0.1107	4099.97	15948.79	79.5
	EL_4	-0.0791	2740.01	8144.34	74.8
	EL_5	-0.0590	1949.99	4525.07	69.9
E=5000 kN/m^2	EL_1	-0.1332	12600.19	46202.00	78.6
	EL_2	-0.0758	6709.94	14954.65	69.0
	EL_3	-0.0480	4099.97	5990.84	59.3
	EL_4	-0.0326	2740.01	2766.03	50.2
	EL_5	-0.0232	1949.99	1405.63	41.9
E=15000 kN/m^2	EL_1	-0.0074	12600.19	464.06	3.56
	EL_2	-0.0034	6709.94	101.21	1.49
	EL_3	-0.0020	4099.97	34.30	0.83
	EL_4	-0.0013	2740.01	15.50	0.56
	EL_5	-0.0010	1949.99	8.48	0.43
E=20000 kN/m^2	EL_1	0	12600.19	0	0
	EL_2	0	6709.94	0	0
	EL_3	0	4099.97	0	0
	EL_4	0	2740.01	0	0
	EL_5	0	1949.99	0	0
E=30000 kN/m^2	EL_1	0	12600.19	0	0
	EL_2	0	6709.94	0	0
	EL_3	0	4099.97	0	0
	EL_4	0	2740.01	0	0
	EL_5	0	1949.99	0	0
E=40000 kN/m^2	EL_1	0	12600.19	0	0
	EL_2	0	6709.94	0	0
	EL_3	0	4099.97	0	0
	EL_4	0	2740.01	0	0
	EL_5	0	1949.99	0	0

Table 4.4: Average of Compaction Energies Lost for 15 cm subgrade

Stiffness of the lower layer, E (kN/m^2)	Average Compaction Energy Loss (%)
E=2500	79.3
E=5000	59.8
E=10000 (homogenous subgrade)	22.0
E=15000	1.37
E=20000	0
E=30000	0
E=40000	0

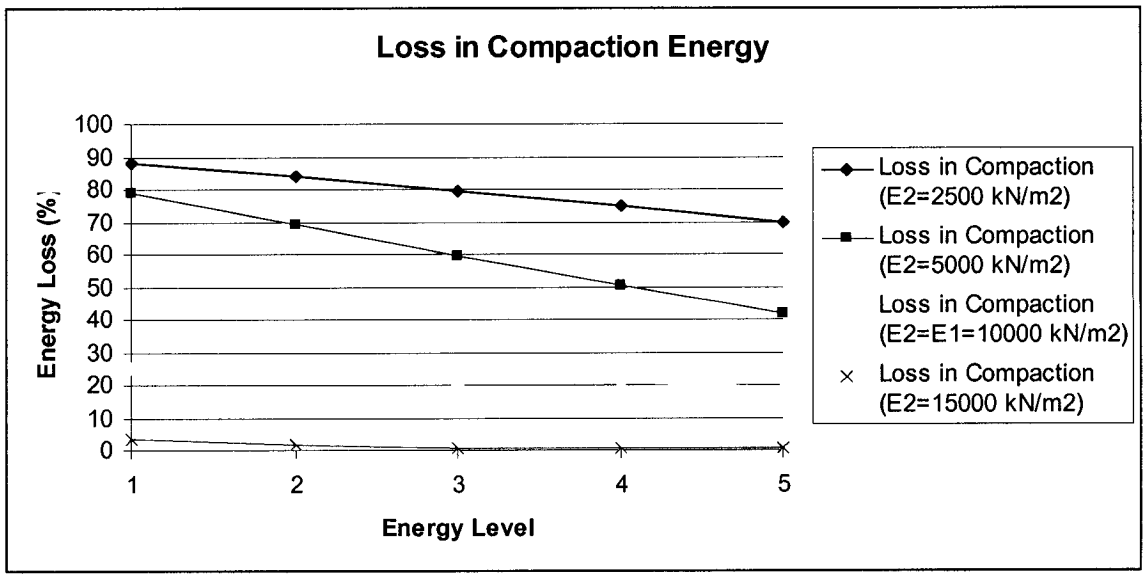

Figure 4.6: Loss in Compaction Energy for different energy and stiffness levels when H=15 cm

Following conclusions can be drawn for the compaction of subgrade when the lower layer is directly underlying the target compaction depth of the subgrade (H=15cm). This is the most critical case for the problem.

a. The amount of the energy lost due to the lower layer is increasing as the stiffness of the lower layer is decreasing.

b. There is no energy loss for E_2= 20000 kN/m^2 and higher. Lower layer starts to absorb some energy as its stiffness is 15000 kN/m^2 and below.

c. A critical stiffness value for the lower layer can be pronounced at the stiffness of E_2=E_1=10000 kN/m^2, where the subgrade is a homogenous layer to an infinite depth. This stiffness value governs the punching effect to the lower layer. Higher and below this value represent two different cases for the dynamic problem; weak layer overlying strong deposit and strong layer overlying weak deposit.

d. For the loss of compaction energy, the percentage of energy lost is greater for higher energy levels when the underlying soil is weak. The difference is as high as 35-40 percent for E_2= 5000 kN/m^2. On the other hand, the percentage of loss of energy is slightly increasing when energy level is decreasing for the case of a stiffer lower layer.

Table 4.5: Deformation and energy values for 0.30 m subgrade

Lower layer stiffness	Energy Level	Deformation at element-a (m)	Deformation at element-b (m)	Energy Taken by the upper layer (Nm)	Energy lost due to lower layer (Nm)	Loss in Compaction (%)
E=2500 kN/m^2	EL_1	-0.1184	-0.1406	12600.19	25731.94	67.2
	EL_2	-0.0708	-0.0865	6709.94	9746.16	59.2
	EL_3	-0.0483	-0.0598	4099.97	4656.53	53.1
	EL_4	-0.0353	-0.0443	2740.01	2553.73	48.2
	EL_5	-0.0270	-0.0343	1949.99	1532.49	44.0
E=5000 kN/m^2	EL_1	-0.0672	-0.0857	12600.19	19127.44	60.3
	EL_2	-0.0385	-0.0513	6709.94	6865.18	50.6
	EL_3	-0.0248	-0.0343	4099.97	3066.89	42.8
	EL_4	-0.0176	-0.0248	2740.01	1602.31	36.9
	EL_5	-0.0132	-0.0189	1949.99	927.22	32.2
E=15000 kN/m^2	EL_1	-0.0098	-0.0133	12600.19	1518.26	10.8
	EL_2	-0.0058	-0.0076	6709.94	489.74	6.80
	EL_3	-0.0043	-0.0051	4099.97	226.16	5.22
	EL_4	-0.0032	-0.0038	2740.01	120.91	4.23
	EL_5	-0.0025	-0.0029	1949.99	69.93	3.46
E=20000 kN/m^2	EL_1	-0.0042	-0.0044	12600.19	217.66	1.70
	EL_2	-0.0033	-0.0031	6709.94	109.55	1.61
	EL_3	-0.0028	-0.0025	4099.97	70.10	1.68
	EL_4	-0.0023	-0.0019	2740.01	41.12	1.48
	EL_5	-0.0019	-0.0015	1949.99	26.10	1.32
E=30000 kN/m^2	EL_1	-0.0011	0.0000	12600.19	6.49	0.0516
	EL_2	-0.0015	-0.0005	6709.94	10.44	0.155
	EL_3	-0.0015	-0.0005	4099.97	9.40	0.229
	EL_4	-0.0013	-0.0004	2740.01	7.31	0.266
	EL_5	-0.0012	-0.0003	1949.99	5.71	0.292
E=40000 kN/m^2	EL_1	-0.0009	0.0000	12600.19	4.77	0.0379
	EL_2	-0.0012	0.0000	6709.94	8.23	0.123
	EL_3	-0.0013	-0.0001	4099.97	7.38	0.180
	EL_4	-0.0012	-0.0001	2740.01	6.44	0.235
	EL_5	-0.0011	-0.0001	1949.99	5.47	0.280

Table 4.6: Average of Compaction Energies Lost for 30 cm subgrade

Stiffness of the lower layer, E (kN/m^2)	Average Compaction Energy Loss (%)
E= 2500	54.4
E= 5000	44.6
E= 10000 (homogenous subgrade)	22.0
E= 15000	6.1
E= 20000	1.56
E= 30000	0.199
E= 40000	0.171

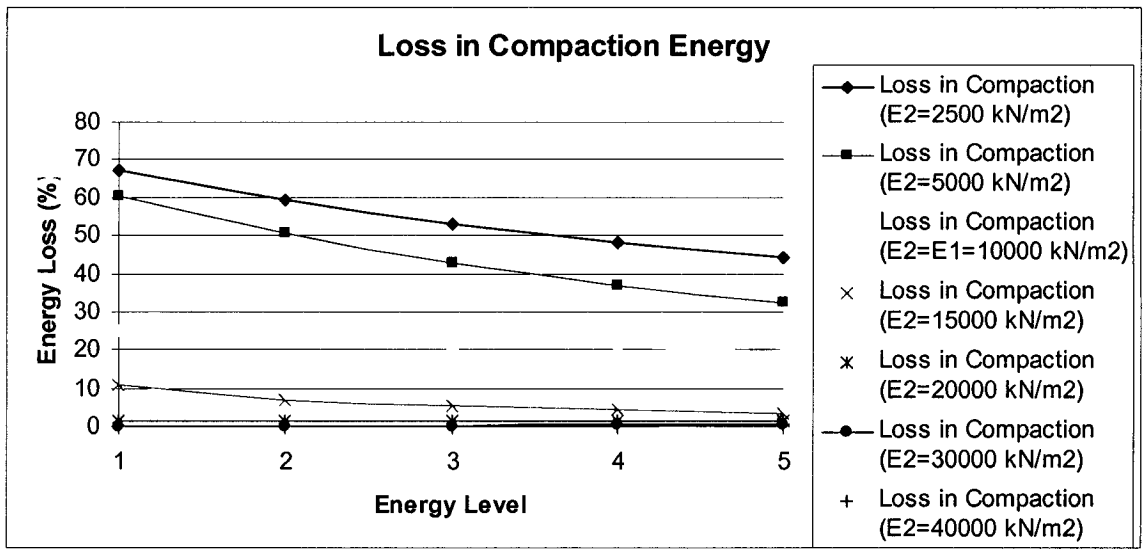

Figure 4.7: Loss in Compaction Energy for different energy and stiffness levels when H=30 cm

Table 4.7: Deformation and energy values for 0.45 m subgrade

Lower layer stiffness	Energy Level	Deformation at element-a (m)	Deformation at element-b (m)	Energy Taken by the upper layer (Nm)	Energy lost due to lower layer (Nm)	Loss in Compaction (%)
E=2500 kN/m^2	EL_1	-0.1012	-0.0882	12600.19	11057.80	46.8
	EL_2	-0.0653	-0.0564	6709.94	4581.45	40.6
	EL_3	-0.0467	-0.0402	4099.97	2336.67	36.3
	EL_4	-0.0353	-0.0301	2740.01	1330.10	32.7
	EL_5	-0.0278	-0.0234	1949.99	819.91	29.6
E= 5000 kN/m^2	EL_1	-0.0653	-0.0588	12600.19	9233.92	42.3
	EL_2	-0.0412	-0.0365	6709.94	3592.39	34.9
	EL_3	-0.0290	-0.0254	4099.97	1749.01	29.9
	EL_4	-0.0221	-0.0191	2740.01	996.00	26.7
	EL_5	-0.0175	-0.0148	1949.99	611.83	23.9
E=15000 kN/m^2	EL_1	-0.0207	-0.0130	12600.19	1768.81	12.3
	EL_2	-0.0141	-0.0080	6709.94	750.75	10.1
	EL_3	-0.0107	-0.0056	4099.97	408.47	9.05
	EL_4	-0.0086	-0.0041	2740.01	254.31	8.49
	EL_5	-0.0072	-0.0031	1949.99	173.34	8.16
E=20000 kN/m^2	EL_1	-0.0163	-0.0061	12600.19	993.75	7.32
	EL_2	-0.0117	-0.0040	6709.94	506.11	7.02
	EL_3	-0.0092	-0.0029	4099.97	312.39	7.07
	EL_4	-0.0076	-0.0022	2740.01	213.20	7.22
	EL_5	-0.0065	-0.0017	1949.99	158.19	7.50
E=30000 kN/m^2	EL_1	-0.0113	-0.0018	12600.19	552.86	4.21
	EL_2	-0.0090	-0.0014	6709.94	349.64	4.95
	EL_3	-0.0075	-0.0010	4099.97	249.60	5.73
	EL_4	-0.0064	-0.0007	2740.01	185.91	6.36
	EL_5	-0.0056	-0.0005	1949.99	145.62	6.95
E=40000 kN/m^2	EL_1	-0.0097	0.0000	12600.19	518.41	3.96
	EL_2	-0.0081	-0.0002	6709.94	338.85	4.81
	EL_3	-0.0070	-0.0003	4099.97	245.77	5.65
	EL_4	-0.0061	-0.0003	2740.01	190.69	6.51
	EL_5	-0.0054	-0.0002	1949.99	152.41	7.25

Table 4.8: Average of Compaction Energies Lost for 45 cm subgrade

Stiffness of the lower layer, E (kN/m^2)	Average Compaction Energy Loss (%)
E= 2500	37.2
E= 5000	31.5
E= 10000 (homogenous subgrade)	22.0
E= 15000	9.62
E= 20000	7.23
E= 30000	5.64
E= 40000	5.63

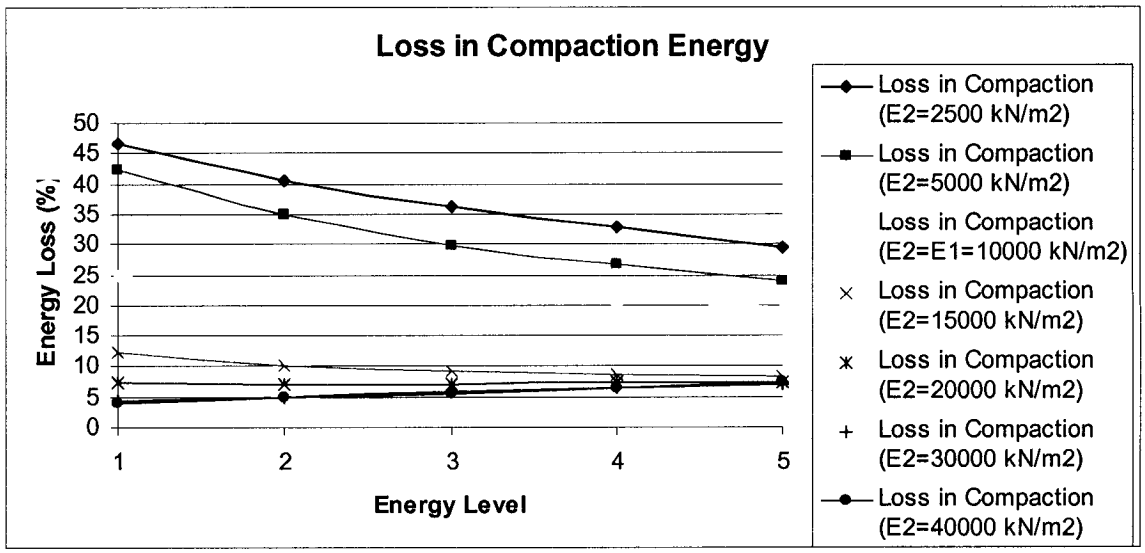

Figure 4.8: Loss in Compaction Energy for different energy and stiffness levels when H=45 cm

Table 4.9: Deformation and energy values for 0.60 m subgrade

Lower layer stiffness	Energy Level	Deformation at element-a (m)	Deformation at element-b (m)	Energy Taken by the upper layer (Nm)	Energy lost due to lower layer (Nm)	Loss in Compaction (%)
E= 2500 kN/m^2	EL_1	-0.0914	-0.0667	12600.19	9142.19	42.1
	EL_2	-0.0606	-0.0429	6709.94	4127.90	38.1
	EL_3	-0.0434	-0.0304	4099.97	2132.13	34.2
	EL_4	-0.0324	-0.0226	2740.01	1196.39	30.4
	EL_5	-0.0252	-0.0173	1949.99	731.68	27.3
E= 5000 kN/m^2	EL_1	-0.0635	-0.0466	12600.19	7232.97	36.5
	EL_2	-0.0412	-0.0295	6709.94	3014.05	31.0
	EL_3	-0.0293	-0.0208	4099.97	1523.46	27.1
	EL_4	-0.0221	-0.0153	2740.01	862.61	23.9
	EL_5	-0.0173	-0.0117	1949.99	527.94	21.3
E= 15000 kN/m^2	EL_1	-0.0284	-0.0123	12600.19	2725.33	17.8
	EL_2	-0.0197	-0.0077	6709.94	1294.85	16.2
	EL_3	-0.0148	-0.0053	4099.97	731.07	15.1
	EL_4	-0.0116	-0.0038	2740.01	460.11	14.4
	EL_5	-0.0096	-0.0028	1949.99	318.46	14.0
E= 20000 kN/m^2	EL_1	-0.0235	-0.0068	12600.19	2052.97	14.0
	EL_2	-0.0169	-0.0044	6709.94	1078.27	13.8
	EL_3	-0.0130	-0.0031	4099.97	651.24	13.7
	EL_4	-0.0105	-0.0022	2740.01	433.02	13.6
	EL_5	-0.0088	-0.0016	1949.99	315.04	13.9
E= 30000 kN/m^2	EL_1	-0.0188	-0.0026	12600.19	1552.53	11.0
	EL_2	-0.0143	-0.0017	6709.94	916.94	12.0
	EL_3	-0.0113	-0.0011	4099.97	592.38	12.6
	EL_4	-0.0093	-0.0008	2740.01	412.85	13.1
	EL_5	-0.0080	-0.0006	1949.99	308.19	13.6
E= 40000 kN/m^2	EL_1	-0.0171	-0.0007	12600.19	1486.33	10.6
	EL_2	-0.0131	-0.0006	6709.94	872.08	11.5
	EL_3	-0.0105	-0.0004	4099.97	561.17	12.0
	EL_4	-0.0087	-0.0003	2740.01	393.43	12.6
	EL_5	-0.0075	-0.0002	1949.99	295.49	13.2

Table 4.10: Average of Compaction Energies Lost for 60 cm subgrade

Stiffness of the lower layer, E (kN/m^2)	Average Compaction Energy Loss (%)
E= 2500	34.4
E= 5000	28.0
E= 10000 (homogenous subgrade)	22.0
E= 15000	15.5
E= 20000	13.8
E= 30000	12.5
E= 40000	12.0

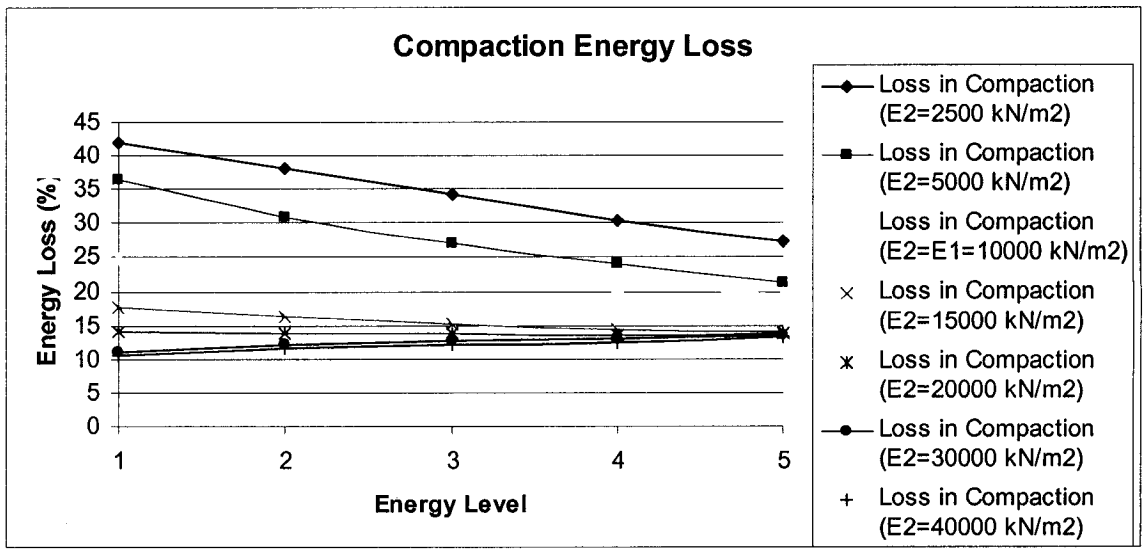

Figure 4.9: Loss in Compaction Energy for different energy and stiffness levels when H=60 cm

Table 4.11: Deformation and energy values for 0.75 m subgrade

Lower layer stiffness	Energy Level	Deformation at element-a (m)	Deformation at element-b (m)	Energy Taken by the upper layer (Nm)	Energy lost due to lower layer (Nm)	Loss in Compaction (%)
E= 2500 kN/m^2	EL_1	-0.0767	-0.0528	12600.19	6775.65	35.0
	EL_2	-0.0500	-0.0335	6709.94	2965.26	30.7
	EL_3	-0.0353	-0.0234	4099.97	1496.38	26.7
	EL_4	-0.0265	-0.0170	2740.01	869.17	24.1
	EL_5	-0.0207	-0.0129	1949.99	553.40	22.1
E= 5000 kN/m^2	EL_1	-0.0564	-0.0386	12600.19	5619.66	30.9
	EL_2	-0.0367	-0.0237	6709.94	2387.66	26.3
	EL_3	-0.0262	-0.0162	4099.97	1230.19	23.1
	EL_4	-0.0199	-0.0117	2740.01	720.60	20.8
	EL_5	-0.0158	-0.0088	1949.99	474.58	19.6
E= 15000 kN/m^2	EL_1	-0.0304	-0.0110	12600.19	3103.56	19.8
	EL_2	-0.0215	-0.0066	6709.94	1588.76	19.1
	EL_3	-0.0165	-0.0044	4099.97	969.71	19.1
	EL_4	-0.0134	-0.0031	2740.01	663.48	19.5
	EL_5	-0.0113	-0.0023	1949.99	490.01	20.1
E= 20000 kN/m^2	EL_1	-0.0270	-0.0066	12600.19	2782.23	18.1
	EL_2	-0.0196	-0.0041	6709.94	1517.25	18.4
	EL_3	-0.0153	-0.0027	4099.97	957.71	18.9
	EL_4	-0.0126	-0.0019	2740.01	666.80	19.6
	EL_5	-0.0107	-0.0014	1949.99	494.08	20.2
E= 30000 kN/m^2	EL_1	-0.0237	-0.0025	12600.19	2576.99	17.0
	EL_2	-0.0177	-0.0016	6709.94	1471.29	18.0
	EL_3	-0.0140	-0.0011	4099.97	945.67	18.7
	EL_4	-0.0116	-0.0008	2740.01	660.78	19.4
	EL_5	-0.0099	-0.0005	1949.99	488.72	20.0
E= 40000 kN/m^2	EL_1	-0.0220	-0.0009	12600.19	2467.90	16.4
	EL_2	-0.0164	-0.0005	6709.94	1398.07	17.2
	EL_3	-0.0131	-0.0003	4099.97	901.60	18.0
	EL_4	-0.0109	-0.0002	2740.01	629.35	18.7
	EL_5	-0.0094	-0.0002	1949.99	466.29	19.3

Table 4.12: Average of Compaction Energies Lost for 75 cm subgrade

Stiffness of the lower layer, E (kN/m^2)	Average Compaction Energy Loss (%)
E= 2500	27.7
E= 5000	24.1
E= 10000 (homogenous subgrade)	22.0
E= 15000	19.5
E= 20000	19.1
E= 30000	18.6
E= 40000	17.9

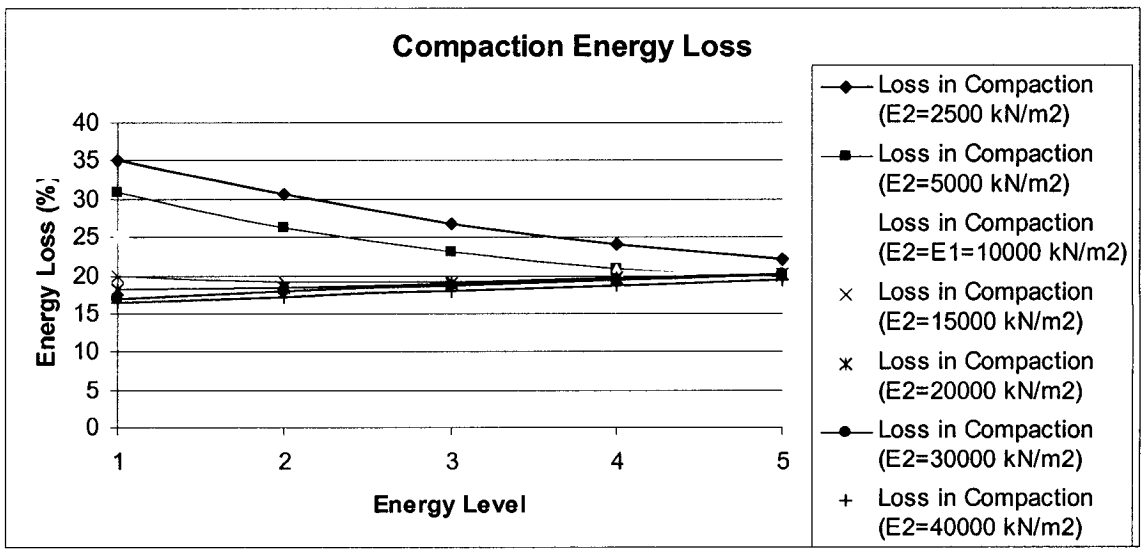

Figure 4.10: Loss in Compaction Energy for different energy and stiffness levels when H=75 cm

Table 4.13: Averages of Percentage of Energy Loss in Compaction for various depths of the subgrade and various stiffness levels of the lower layer

Stiffness of the lower layer, E_2 (kN/m^2)	**Loss in Compaction Energy (%)**				
	Depth of Subgrade				
	15 cm	*30 cm*	*45 cm*	*60 cm*	*75 cm*
2500	79.3	54.4	37.2	34.4	***27.7***
5000	59.8	44.6	31.5	28	***24.1***
10000 (homogenous case)					***22***
15000	1.37	6.1	9.62	15.5	***19.5***
20000	0	1.56	7.23	13.8	***19.1***
30000	0	0.199	5.64	12.5	***18.6***
40000	0	0.171	5.63	12	***17.9***

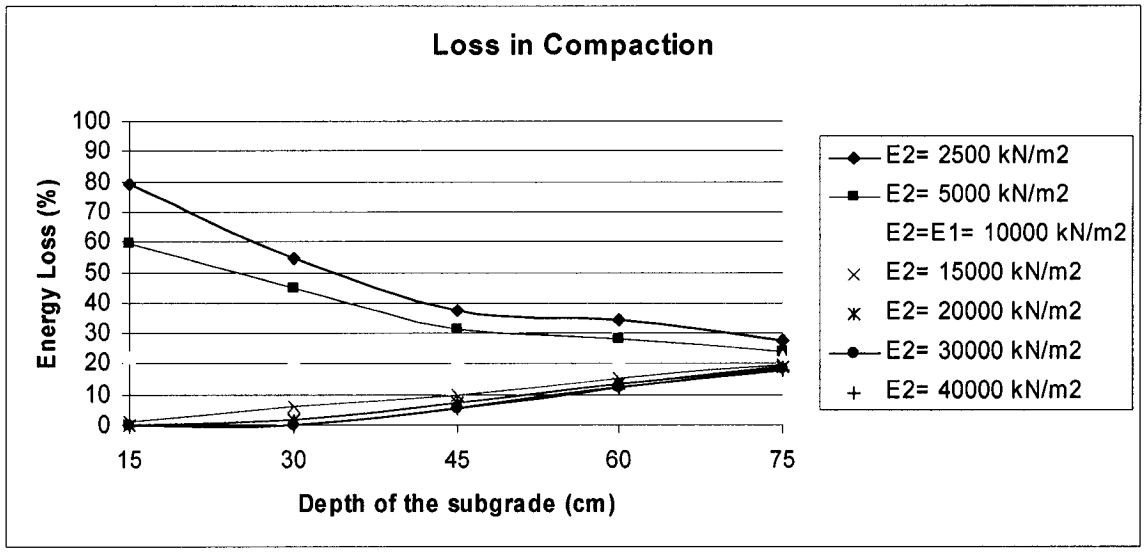

Figure 4.11: Values of Energy Loss for different stiffness of the lower layer and subgrade depth levels

Figure 4.11 shows a general result of the combined effect of depth of subgrade and stiffness level of the lower layer. The percentages of "energy loss" values on the y-axis are the average energy loss values for all energy levels used in this study. When curve fitting technique is applied on the curves obtained in the above graph, a correlation between the stiffness of the lower layer and the percentage of compaction energy loss for different depths of the subgrade is obtained. The R^2 value calculated is close to 1.0 when a second order polynomial equation is suggested.

Table 4.14 shows the coefficients a, b, and c for the mentioned polynomial formulation. These coefficients may be used for a preliminary estimation of the percentage of compaction energy loss when the stiffness of the lower layer and the thickness of the subgrade are known. It should be mentioned that these values are for a

subgrade having a stiffness value 10000 kN/m^2 and a poisson's ratio of 0.3; representing average loose granular material that is often used as the subgrade in most of the cases.

$$Compaction\ Energy\ Loss = aT_s^2 + bT_s + c \quad \text{..... (4.3)}$$

Where; a, b, and c are coefficients for stiffness of the lower layer and T_s is the thickness of the subgrade layer.

Table 4.14: Coefficients for estimating average loss in compaction energy for different stiffness values of the lower layer

Stiffness of the lower layer, E_2 (kN/m2)	**Coefficient-a**	**Coefficient-b**	**Coefficient-c**	**R^2**
2500	0.0161	-2.2728	108.96	0.987
5000	0.0102	-1.5067	80.1	0.994
15000	0.0003	0.2787	-2.83	0.996
20000	0.0027	0.0968	-2.604	0.989
30000	0.0042	-0.0477	-0.85	0.986
40000	0.0039	-0.0359	-0.964	0.986

Following conclusions can be drawn in general for results of analyses:

a. The non-homogeneous subgrade-lower layer system starts to behave as a homogeneous subgrade layer after a subgrade depth of 75 cm that coincides with 5 times the target depth of compaction. This can be observed by tightly placed energy loss curves in figure 4.11.

b. The loss in compaction energy for stiffer lower layer is increasing as the depth of the subgrade layer is increased. For weaker subgrade, the situation is opposite; loss in energy is decreasing by increasing subgrade depth.

c. Energy loss in the case of the presence of a weak lower layer is critical up to 45cm subgrade thickness, which is 3 times the target depth of compaction. As the thickness is increased from 45cm to higher values, the rate of energy loss is decreasing (refer to figure 4.11).

4.8 DISSIPATION OF ENERGY TO THE LOWER LAYER

The analyses performed so far have concluded that there is loss of compaction energy when the subgrade to be compacted is underlain by a weak deep deposit, whose mechanism is controlled by the stiffness of the lower layer and depth of the subgrade. In that regard, it is already shown that the actual site conditions play an important role on the compaction of a thin subgrade when compared with the small-scale test conditions used in Proctor test. It should be mentioned again that, the results obtained to this point are reflecting the behavior of compaction process and combined effect of subgrade depth and lower layer stiffness for one pass of compaction only.

In this part of the numerical analysis, it is aimed to determine the behavior of the energy loss phenomenon over a longer period of time that is to say to the possible end of a compaction project. For this purpose, an energy level equal to the energy level used in Proctor Test will be applied by means of successive drops onto the two-layer system. With reference to the analyses concluded so far, the lower layer stiffness would be taken lower than that of the subgrade, revealing the case of strong layer overlying deep weak deposit in which the compaction energy loss was found to be significant.

Figure 4.12 show the loading-unloading cycles for 24-drop analyses to be done in the proceeding section. The duration of loading and unloading cycles are taken to be 0.1 and 0.2 second respectively as it has already been used throughout the analyses in this research. Respectively, 24 loading and unloading cycles are carried on for 7.2 seconds in the numerical model. Figure 4.13 shows how the soil is responding to the impact loading

by means of vibrations. Vertical peak particle accelerations at the point of impact reach a peak value after each drop and then descend to zero just before the next impact, the principle being allowing enough unloading time for the soil to recover and rebound from the previous impact.

As shown in the table 4.15, it is calculated that 4 passes of compaction up to 24 drops using energy level 1 (EL_1) will be sufficient to deliver the equal amount of proctor energy per 1 cm^2 of soil through the base of the tamper.

Table 4.15: Calculated Number of Drops and Energy Level for Equivalent Proctor Energy to be used in Field Compaction

Feature	Proctor Test	Field Compaction
Weight of Hammer (kg)	2.6	Variable weight of tamper and height of drop with constant energy level, EL_1 (250 kgm per drop with γ=0.3)
Drop Height (m)	0.31	
Tamper Diameter (m)	0.1	1.0
Number of Drops	75	24.18 ≈24
Total Energy per tamper base area (kgm/m^2)	7696.733	7696.733

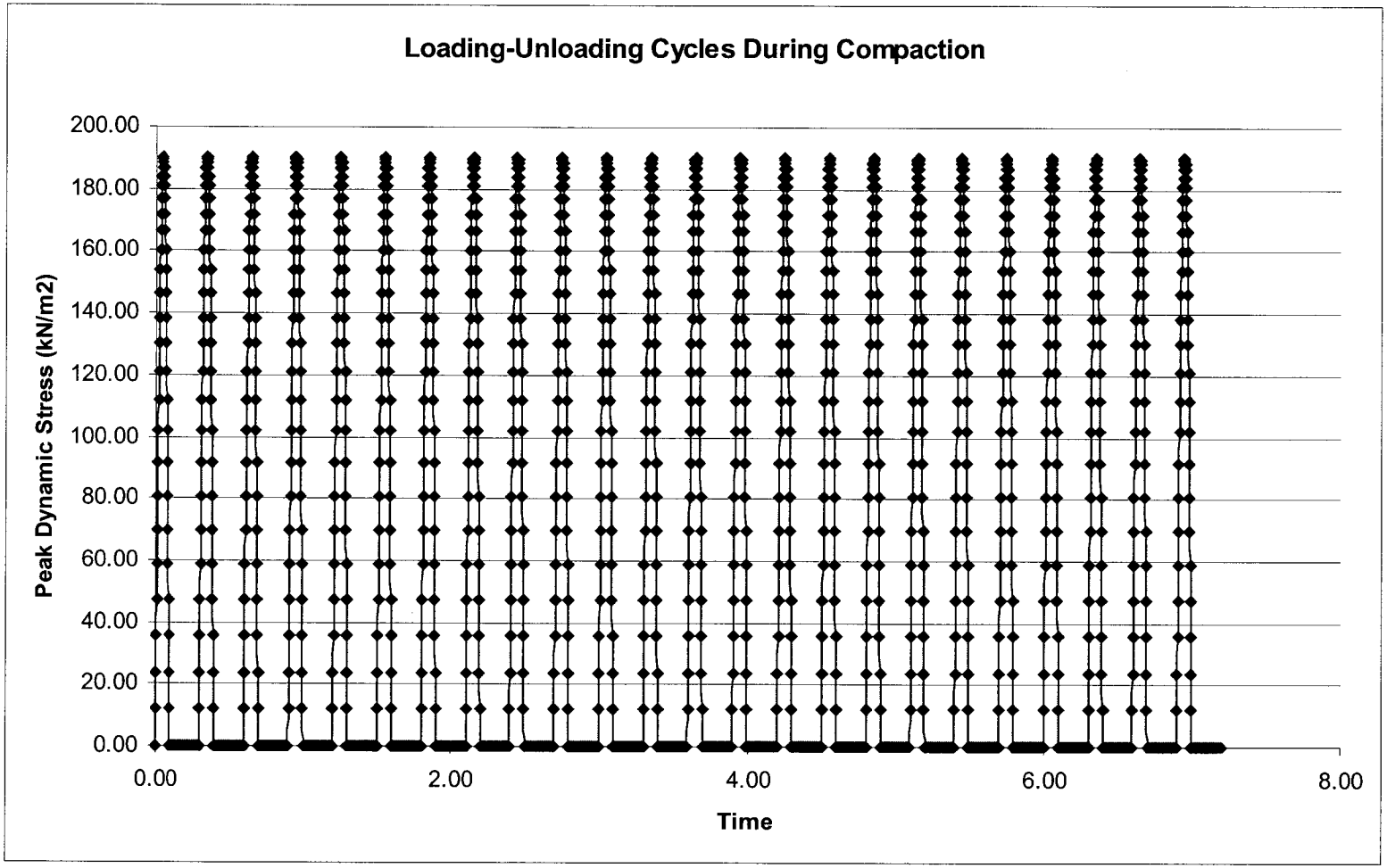

Figure 4.12: Successive Impacts Applied During Compaction Process

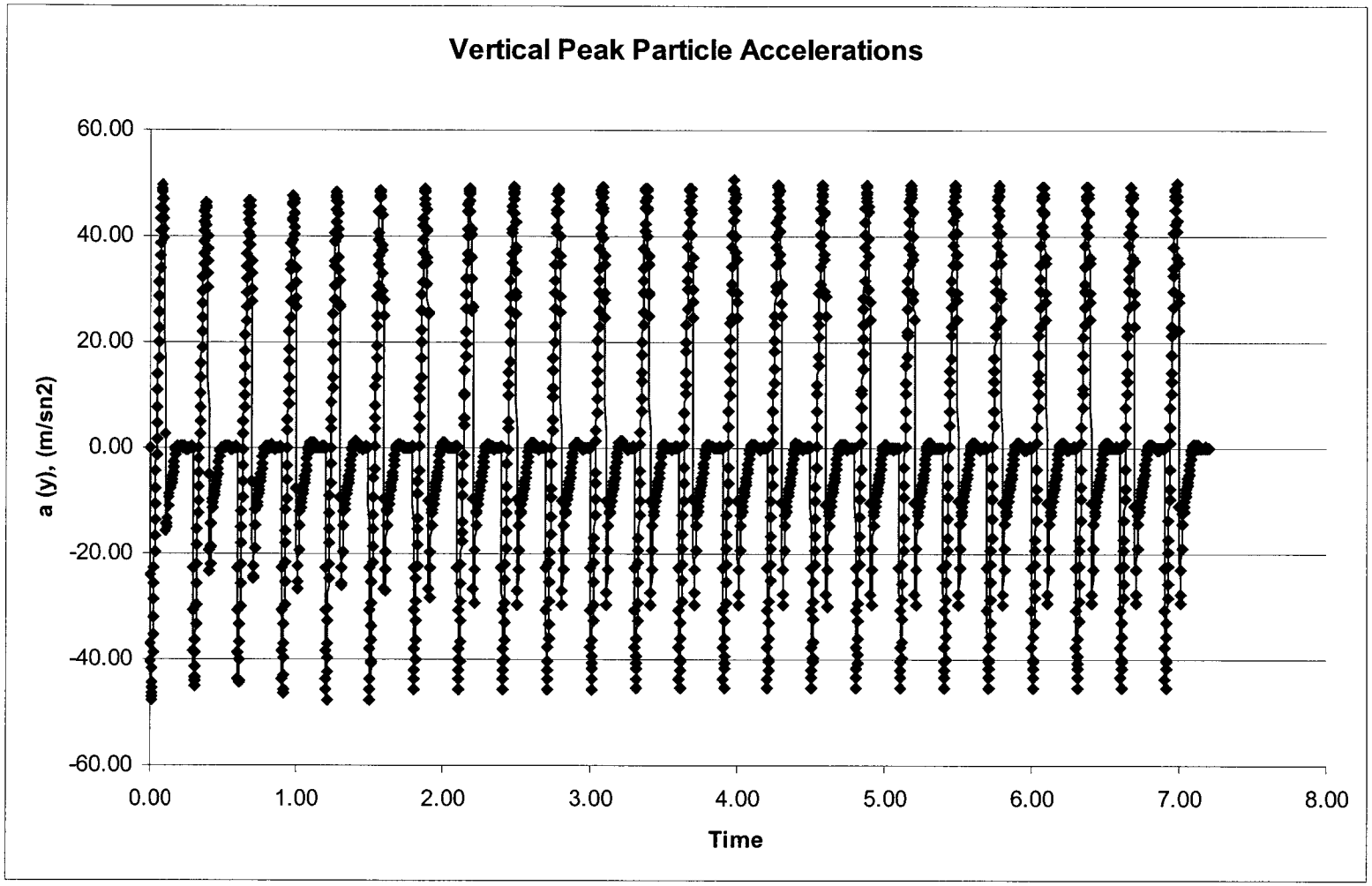

Figure 4.13: Vertical Peak Particle Accelerations after successive impacts

4.9 RESULTS OF ANALYSIS UP TO 24 DROPS OF COMPACTION

Table 4.16: Deformation and energy values for homogenous subgrade during compaction process

Drop Number	Deformation at the point of impact (m)	Deformation at element-a (m)	Energy taken by the target depth (cumulative) (Nm)	Energy lost below the target depth (cumulative) (Nm)	Loss in compaction (%)
1	-0.0287	-0.0144	3373.57	1146.03	25.4
2	-0.0380	-0.0194	5886.12	2064.05	26.0
3	-0.0441	-0.0224	7896.63	2766.14	25.9
4	-0.0486	-0.0246	9627.45	3326.98	25.7
5	-0.0522	-0.0263	11181.69	3792.67	25.3
6	-0.0553	-0.0276	12617.66	4190.92	24.9
7	-0.0580	-0.0287	13963.95	4537.91	24.5
8	-0.0605	-0.0297	15240.69	4844.49	24.1
9	-0.0627	-0.0305	16459.53	5118.59	23.7
10	-0.0647	-0.0313	17632.43	5366.69	23.3
11	-0.0666	-0.0319	18762.93	5593.45	23.0
12	-0.0683	-0.0325	19857.73	5801.66	22.6
13	-0.0700	-0.0330	20919.67	5991.30	22.3
14	-0.0716	-0.0335	21959.96	6169.29	21.9
15	-0.0730	-0.0340	22974.91	6334.30	21.6
16	-0.0745	-0.0344	23971.77	6489.08	21.3
17	-0.0758	-0.0347	24950.93	6634.86	21.0
18	-0.0771	-0.0351	25908.85	6770.30	20.7
19	-0.0784	-0.0354	26856.14	6898.64	20.4
20	-0.0796	-0.0357	27796.51	7021.69	20.2
21	-0.0808	-0.0360	28725.86	7137.71	19.9
22	-0.0820	-0.0363	29650.51	7251.78	19.7
23	-0.0831	-0.0366	30572.99	7361.57	19.4
24	-0.0842	-0.0369	31498.46	7469.87	19.2

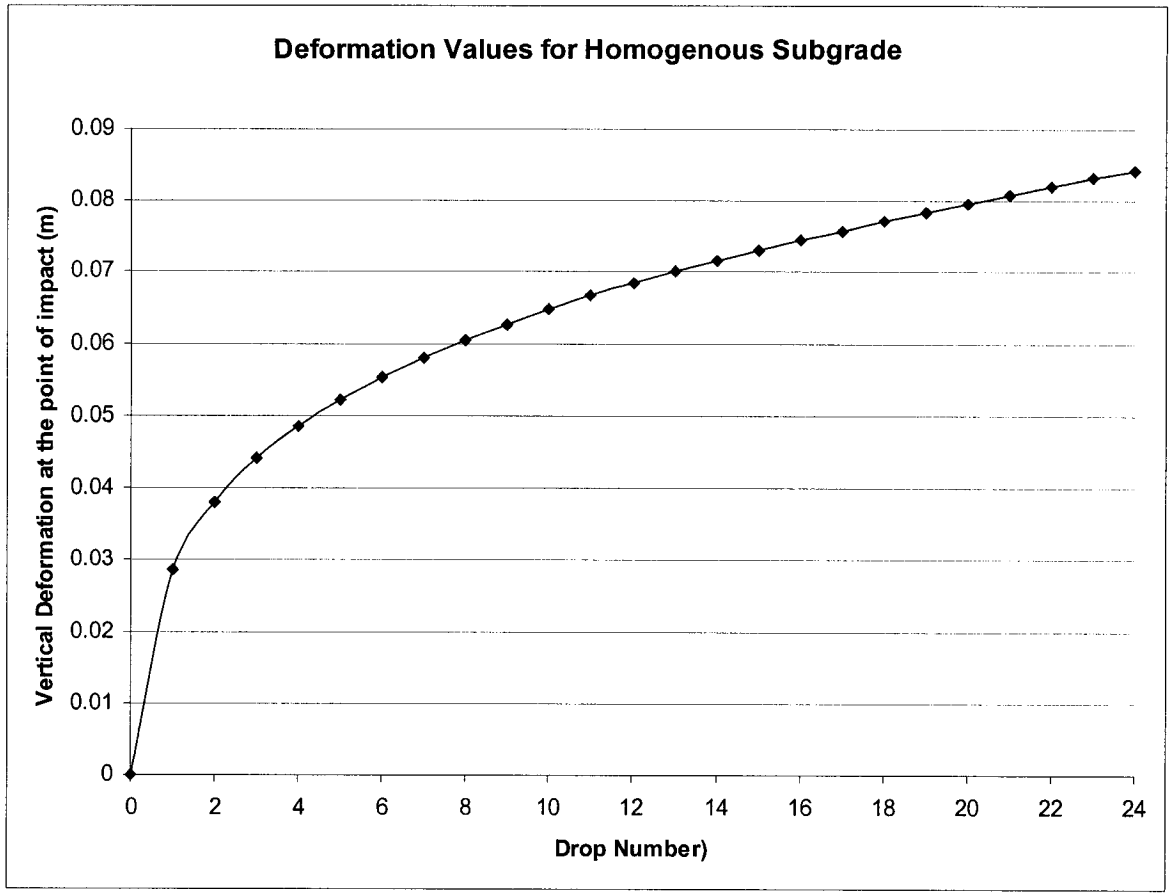

Figure 4.14: Vertical Deformation over time for homogenous subgrade upon impact

Figure 4.14 shows the depth of crater formation at the point of impact. It should be noted that the rate of increasing of this depth is decreasing as compaction is continued. The same behavior in the overall compaction of the homogenous subgrade may be expected, where there will be no additional compaction after the crater depth reaches a peak value.

Table 4.17: Deformation and energy values for 0.15 m subgrade (target depth=subgrade depth) underlain by lower layer-1 (E_2=2500 KN/m^2)

Drop Number	Deformation at element-a (m)	Energy taken by the upper layer (cumulative) (Nm)	Energy lost to the lower layer (cumulative) (Nm)	Loss in compaction (%)
1	-0.0715	3373.57	6658.77	66.4
2	-0.1197	5886.12	18654.58	76.0
3	-0.1613	7896.63	33893.82	81.1
4	-0.2001	9627.45	52117.86	84.4
5	-0.2370	11181.69	73152.85	86.7
6	-0.2670	12617.66	92824.23	88.0
7	-0.3077	13963.95	123276.97	89.8
8	-0.3419	15240.69	152244.86	90.9
9	-0.3757	16459.53	183746.57	91.8
10	-0.4089	17632.43	217752.60	92.5
11	-0.4419	18762.93	254250.69	93.1
12	-0.4746	19857.73	293248.11	93.7
13	-0.5070	20919.67	334745.30	94.1
14	-0.5393	21959.96	378742.23	94.5
15	-0.5715	22974.91	425251.26	94.9
16	-0.6035	23971.77	474283.70	95.2
17	-0.6355	24950.93	525828.93	95.5
18	-0.6673	25908.85	579872.26	95.7
19	-0.6991	26856.14	636425.70	96.0
20	-0.7308	27796.51	695473.66	96.2
21	-0.7625	28725.86	757007.49	96.3
22	-0.7941	29650.51	821017.79	96.5
23	-0.8256	30572.99	887497.34	96.7
24	-0.8571	31498.46	956437.18	96.8

Table 4.18: Deformation and energy values for 0.15 m subgrade (target depth=subgrade depth) underlain by lower layer-2 (E_2=5000 KN/m^2)

Drop Number	Deformation at element-a (m)	Energy taken by the upper layer (cumulative) (Nm)	Energy lost to the lower layer (cumulative) (Nm)	Loss in compaction (%)
1	-0.0419	3373.57	4563.84	57.5
2	-0.0660	5886.12	11345.31	65.8
3	-0.0861	7896.63	19297.56	71.0
4	-0.1042	9627.45	28275.58	74.6
5	-0.1211	11181.69	38220.91	77.4
6	-0.1330	12617.66	46065.10	78.5
7	-0.1529	13963.95	60858.21	81.3
8	-0.1680	15240.69	73535.89	82.8
9	-0.1829	16459.53	87127.62	84.1
10	-0.1976	17632.43	101645.87	85.2
11	-0.2120	18762.93	117096.00	86.2
12	-0.2264	19857.73	133486.20	87.1
13	-0.2407	20919.67	150822.30	87.8
14	-0.2548	21959.96	169113.42	88.5
15	-0.2689	22974.91	188368.35	89.1
16	-0.2830	23971.77	208590.41	89.7
17	-0.2970	24950.93	229781.72	90.2
18	-0.3110	25908.85	251941.43	90.7
19	-0.3250	26856.14	275071.76	91.1
20	-0.3389	27796.51	299170.01	91.5
21	-0.3529	28725.86	324239.56	91.9
22	-0.3667	29650.51	350273.83	92.2
23	-0.3806	30572.99	377268.69	92.5
24	-0.3945	31498.46	405226.51	92.8

Table 4.19: Deformation and energy values for 0.30 m subgrade underlain by lower layer-1 (E_2=2500 KN/m^2)

Drop Number	Deformation at element-a (m)	Deformation at element-b (m)	Energy taken by the upper layer (cumulative) (Nm)	Energy lost to the lower layer (cumulative) (Nm)	Loss in compaction (%)
1	-0.0413	-0.0475	3373.57	2934.88	46.5
2	-0.0632	-0.0750	5886.12	7320.53	55.4
3	-0.0797	-0.0963	7896.63	12080.91	60.5
4	-0.0932	-0.1144	9627.45	17028.92	63.9
5	-0.1050	-0.1304	11181.69	22152.54	66.5
6	-0.1184	-0.1406	12617.66	25731.94	67.1
7	-0.1252	-0.1588	13963.95	32840.77	70.2
8	-0.1341	-0.1716	15240.69	38358.91	71.6
9	-0.1423	-0.1838	16459.53	43977.34	72.8
10	-0.1501	-0.1953	17632.43	49688.52	73.8
11	-0.1574	-0.2064	18762.93	55483.76	74.7
12	-0.1642	-0.2171	19857.73	61358.41	75.6
13	-0.1708	-0.2273	20919.67	67297.20	76.3
14	-0.1770	-0.2373	21959.96	73295.86	77.0
15	-0.1830	-0.2470	22974.91	79410.25	77.6
16	-0.1888	-0.2565	23971.77	85663.13	78.1
17	-0.1945	-0.2659	24950.93	92059.43	78.7
18	-0.2001	-0.2752	25908.85	98602.25	79.2
19	-0.2056	-0.2844	26856.14	105297.93	79.7
20	-0.2110	-0.2935	27796.51	112145.15	80.1
21	-0.2163	-0.3025	28725.86	119149.05	80.6
22	-0.2216	-0.3115	29650.51	126306.79	81.0
23	-0.2268	-0.3204	30572.99	133627.81	81.4
24	-0.2319	-0.3292	31498.46	141115.80	81.8

Table 4.20: Deformation and energy values for 0.30 m subgrade underlain by lower layer-2 (E_2=5000 KN/m^2)

Drop Number	Deformation at element-a (m)	Deformation at element-b (m)	Energy taken by the upper layer (cumulative) (Nm)	Energy lost to the lower layer (cumulative) (Nm)	Loss in compaction (%)
1	-0.0292	-0.0332	3373.57	2875.43	46.0
2	-0.0423	-0.0500	5886.12	6513.86	52.5
3	-0.0513	-0.0625	7896.63	10183.82	56.3
4	-0.0582	-0.0728	9627.45	13791.90	58.9
5	-0.0638	-0.0815	11181.69	17318.10	60.8
6	-0.0672	-0.0857	12617.66	19127.44	60.3
7	-0.0722	-0.0962	13963.95	24102.84	63.3
8	-0.0757	-0.1026	15240.69	27401.62	64.3
9	-0.0786	-0.1085	16459.53	30644.63	65.1
10	-0.0813	-0.1140	17632.43	33840.82	65.7
11	-0.0836	-0.1192	18762.93	36998.29	66.4
12	-0.0857	-0.1241	19857.73	40120.63	66.9
13	-0.0876	-0.1288	20919.67	43209.73	67.4
14	-0.0892	-0.1333	21959.96	46286.38	67.8
15	-0.0908	-0.1377	22974.91	49385.87	68.3
16	-0.0923	-0.1420	23971.77	52523.01	68.7
17	-0.0937	-0.1462	24950.93	55698.18	69.1
18	-0.0950	-0.1504	25908.85	58914.47	69.5
19	-0.0963	-0.1545	26856.14	62176.13	69.8
20	-0.0975	-0.1586	27796.51	65483.30	70.2
21	-0.0986	-0.1626	28725.86	68841.07	70.6
22	-0.0998	-0.1666	29650.51	72251.91	70.9
23	-0.1009	-0.1705	30572.99	75724.71	71.2
24	-0.1020	-0.1745	31498.46	79254.55	71.6

Table 4.21: Deformation and energy values for 0.45 m subgrade underlain by lower layer-1 (E_2=2500 KN/m^2)

Drop Number	Deformation at element-a (m)	Deformation at element-b (m)	Energy taken by the upper layer (cumulative) (Nm)	Energy lost to the lower layer (cumulative) (Nm)	Loss in compaction (%)
1	-0.0372	-0.0363	3373.57	1722.64	33.8
2	-0.0572	-0.0567	5886.12	4190.96	41.6
3	-0.0722	-0.0721	7896.63	6767.50	46.2
4	-0.0846	-0.0846	9627.45	9319.38	49.2
5	-0.0951	-0.0952	11181.69	11804.04	51.4
6	-0.1045	-0.1044	12617.66	14203.74	53.0
7	-0.1129	-0.1126	13963.95	16515.04	54.2
8	-0.1205	-0.1200	15240.69	18741.95	55.2
9	-0.1275	-0.1267	16459.53	20891.18	55.9
10	-0.1340	-0.1328	17632.43	22969.56	56.6
11	-0.1401	-0.1385	18762.93	24979.27	57.1
12	-0.1459	-0.1437	19857.73	26924.31	57.6
13	-0.1513	-0.1486	20919.67	28810.89	57.9
14	-0.1565	-0.1533	21959.96	30642.12	58.3
15	-0.1615	-0.1576	22974.91	32422.73	58.5
16	-0.1662	-0.1617	23971.77	34169.29	58.8
17	-0.1708	-0.1657	24950.93	35883.97	59.0
18	-0.1752	-0.1695	25908.85	37572.33	59.2
19	-0.1796	-0.1731	26856.14	39235.26	59.4
20	-0.1837	-0.1766	27796.51	40874.42	59.5
21	-0.1878	-0.1799	28725.86	42487.96	59.7
22	-0.1917	-0.1831	29650.51	44080.33	59.8
23	-0.1956	-0.1863	30572.99	45655.34	59.9
24	-0.1994	-0.1893	31498.46	47208.33	60.0

Table 4.22: Deformation and energy values for 0.45 m subgrade underlain by lower layer-2 (E_2=5000 KN/m^2)

Drop Number	Deformation at element-a (m)	Deformation at element-b (m)	Energy taken by the upper layer (cumulative) (Nm)	Energy lost to the lower layer (cumulative) (Nm)	Loss in compaction (%)
1	-0.0273	-0.0268	3373.57	1870.36	35.7
2	-0.0399	-0.0403	5886.12	4222.75	41.8
3	-0.0488	-0.0497	7896.63	6439.29	44.9
4	-0.0556	-0.0571	9627.45	8501.24	46.9
5	-0.0613	-0.0632	11181.69	10414.62	48.2
6	-0.0660	-0.0684	12617.66	12199.59	49.2
7	-0.0702	-0.0730	13963.95	13869.97	49.8
8	-0.0738	-0.0770	15240.69	15434.19	50.3
9	-0.0771	-0.0806	16459.53	16897.49	50.7
10	-0.0800	-0.0838	17632.43	18273.09	50.9
11	-0.0827	-0.0867	18762.93	19567.43	51.0
12	-0.0852	-0.0894	19857.73	20791.56	51.1
13	-0.0874	-0.0918	20919.67	21949.04	51.2
14	-0.0895	-0.0941	21959.96	23052.76	51.2
15	-0.0914	-0.0962	22974.91	24108.74	51.2
16	-0.0932	-0.0982	23971.77	25124.43	51.2
17	-0.0949	-0.1001	24950.93	26103.92	51.1
18	-0.0965	-0.1019	25908.85	27047.72	51.1
19	-0.0980	-0.1036	26856.14	27954.81	51.0
20	-0.0994	-0.1052	27796.51	28830.68	50.9
21	-0.1007	-0.1068	28725.86	29678.49	50.8
22	-0.1020	-0.1082	29650.51	30497.36	50.7
23	-0.1032	-0.1096	30572.99	31286.38	50.6
24	-0.1043	-0.1109	31498.46	32052.15	50.4

Table 4.23: Deformation and energy values for 0.60 m subgrade underlain by lower layer-1 (E_2=2500 KN/m^2)

Drop Number	Deformation at element-a (m)	Deformation at element-b (m)	Energy taken by the upper layer (cumulative) (Nm)	Energy lost to the lower layer (cumulative) (Nm)	Loss in compaction (%)
1	-0.0351	-0.0274	3373.57	1300.05	27.8
2	-0.0532	-0.0419	5886.12	2985.52	33.7
3	-0.0668	-0.0529	7896.63	4706.15	37.3
4	-0.0779	-0.0617	9627.45	6403.65	39.9
5	-0.0875	-0.0689	11181.69	8072.39	41.9
6	-0.0959	-0.0751	12617.66	9723.25	43.5
7	-0.1036	-0.0804	13963.95	11367.17	44.9
8	-0.1106	-0.0851	15240.69	13013.43	46.1
9	-0.1172	-0.0892	16459.53	14671.97	47.1
10	-0.1234	-0.0929	17632.43	16345.56	48.1
11	-0.1292	-0.0962	18762.93	18040.64	49.0
12	-0.1348	-0.0992	19857.73	19763.09	49.9
13	-0.1401	-0.1020	20919.67	21512.66	50.7
14	-0.1451	-0.1045	21959.96	23298.56	51.5
15	-0.1500	-0.1068	22974.91	25127.20	52.2
16	-0.1548	-0.1089	23971.77	26999.73	53.0
17	-0.1594	-0.1109	24950.93	28918.66	53.7
18	-0.1638	-0.1128	25908.85	30890.88	54.4
19	-0.1682	-0.1145	26856.14	32917.57	55.1
20	-0.1725	-0.1161	27796.51	35007.02	55.7
21	-0.1766	-0.1176	28725.86	37145.33	56.4
22	-0.1807	-0.1190	29650.51	39352.30	57.0
23	-0.1847	-0.1204	30572.99	41610.93	57.6
24	-0.1886	-0.1216	31498.46	43933.20	58.2

Table 4.24: Deformation and energy values for 0.60 m subgrade underlain by lower layer-2 (E_2=5000 KN/m^2)

Drop Number	Deformation at element-a (m)	Deformation at element-b (m)	Energy taken by the upper layer (cumulative) (Nm)	Energy lost to the lower layer (cumulative) (Nm)	Loss in compaction (%)
1	-0.0272	-0.0209	3373.57	1356.00	28.7
2	-0.0394	-0.0314	5886.12	2922.61	33.2
3	-0.0480	-0.0387	7896.63	4377.16	35.7
4	-0.0549	-0.0443	9627.45	5725.80	37.3
5	-0.0608	-0.0488	11181.69	6991.33	38.5
6	-0.0660	-0.0526	12617.66	8188.65	39.4
7	-0.0706	-0.0559	13963.95	9321.17	40.0
8	-0.0748	-0.0587	15240.69	10399.97	40.6
9	-0.0786	-0.0612	16459.53	11429.83	41.0
10	-0.0822	-0.0634	17632.43	12422.78	41.3
11	-0.0856	-0.0654	18762.93	13381.43	41.6
12	-0.0887	-0.0672	19857.73	14309.98	41.9
13	-0.0917	-0.0688	20919.67	15213.31	42.1
14	-0.0945	-0.0703	21959.96	16095.36	42.3
15	-0.0972	-0.0716	22974.91	16951.25	42.5
16	-0.0998	-0.0728	23971.77	17797.90	42.6
17	-0.1022	-0.0739	24950.93	18621.55	42.7
18	-0.1045	-0.0749	25908.85	19439.22	42.9
19	-0.1068	-0.0759	26856.14	20249.22	43.0
20	-0.1090	-0.0768	27796.51	21046.96	43.1
21	-0.1111	-0.0775	28725.86	21843.07	43.2
22	-0.1131	-0.0783	29650.51	22630.96	43.3
23	-0.1151	-0.0790	30572.99	23416.40	43.4
24	-0.1170	-0.0796	31498.46	24200.43	43.4

Table 4.25: Deformation and energy values for 0.75 m subgrade underlain by lower layer-1 (E_2=2500 KN/m^2)

Drop Number	Deformation at element-a (m)	Deformation at element-b (m)	Energy taken by the upper layer (cumulative) (Nm)	Energy lost to the lower layer (cumulative) (Nm)	Loss in compaction (%)
1	-0.0332	-0.0207	3373.57	1411.62	29.5
2	-0.0498	-0.0314	5886.12	3145.65	34.8
3	-0.0622	-0.0391	7896.63	4913.82	38.4
4	-0.0724	-0.0454	9627.45	6686.94	41.0
5	-0.0811	-0.0505	11181.69	8461.34	43.1
6	-0.0888	-0.0549	12617.66	10255.06	44.8
7	-0.0958	-0.0586	13963.95	12072.22	46.4
8	-0.1022	-0.0618	15240.69	13941.05	47.8
9	-0.1081	-0.0645	16459.53	15869.45	49.1
10	-0.1137	-0.0669	17632.43	17879.91	50.3
11	-0.1190	-0.0689	18762.93	19965.59	51.6
12	-0.1241	-0.0707	19857.73	22145.54	52.7
13	-0.1289	-0.0723	20919.67	24418.85	53.9
14	-0.1336	-0.0737	21959.96	26788.31	55.0
15	-0.1382	-0.0749	22974.91	29267.53	56.0
16	-0.1426	-0.0761	23971.77	31833.39	57.0
17	-0.1468	-0.0771	24950.93	34480.56	58.0
18	-0.1510	-0.0779	25908.85	37234.79	59.0
19	-0.1551	-0.0787	26856.14	40083.75	59.9
20	-0.1590	-0.0794	27796.51	43035.54	60.8
21	-0.1629	-0.0801	28725.86	46076.04	61.6
22	-0.1668	-0.0806	29650.51	49251.10	62.4
23	-0.1705	-0.0812	30572.99	52470.71	63.2
24	-0.1743	-0.0816	31498.46	55833.42	63.9

Table 4.26: Deformation and energy values for 0.75 m subgrade underlain by lower layer-2 (E_2=5000 KN/m^2)

Drop Number	Deformation at element-a (m)	Deformation at element-b (m)	Energy taken by the upper layer (cumulative) (Nm)	Energy lost to the lower layer (cumulative) (Nm)	Loss in compaction (%)
1	-0.0274	-0.0160	3373.57	1381.74	29.1
2	-0.0395	-0.0240	5886.12	2813.74	32.3
3	-0.0478	-0.0298	7896.63	4085.09	34.1
4	-0.0542	-0.0341	9627.45	5248.10	35.3
5	-0.0596	-0.0376	11181.69	6340.53	36.2
6	-0.0643	-0.0405	12617.66	7391.07	36.9
7	-0.0686	-0.0428	13963.95	8419.04	37.6
8	-0.0725	-0.0448	15240.69	9437.94	38.2
9	-0.0761	-0.0465	16459.53	10452.69	38.8
10	-0.0796	-0.0480	17632.43	11482.66	39.4
11	-0.0829	-0.0493	18762.93	12523.86	40.0
12	-0.0860	-0.0504	19857.73	13584.81	40.6
13	-0.0890	-0.0514	20919.67	14667.39	41.2
14	-0.0919	-0.0522	21959.96	15771.03	41.8
15	-0.0948	-0.0530	22974.91	16906.86	42.4
16	-0.0975	-0.0536	23971.77	18072.55	43.0
17	-0.1002	-0.0542	24950.93	19263.06	43.6
18	-0.1027	-0.0547	25908.85	20476.80	44.1
19	-0.1053	-0.0551	26856.14	21719.42	44.7
20	-0.1077	-0.0555	27796.51	23003.17	45.3
21	-0.1101	-0.0559	28725.86	24315.72	45.8
22	-0.1125	-0.0562	29650.51	25673.35	46.4
23	-0.1149	-0.0564	30572.99	27058.67	47.0
24	-0.1172	-0.0567	31498.46	28487.25	47.5

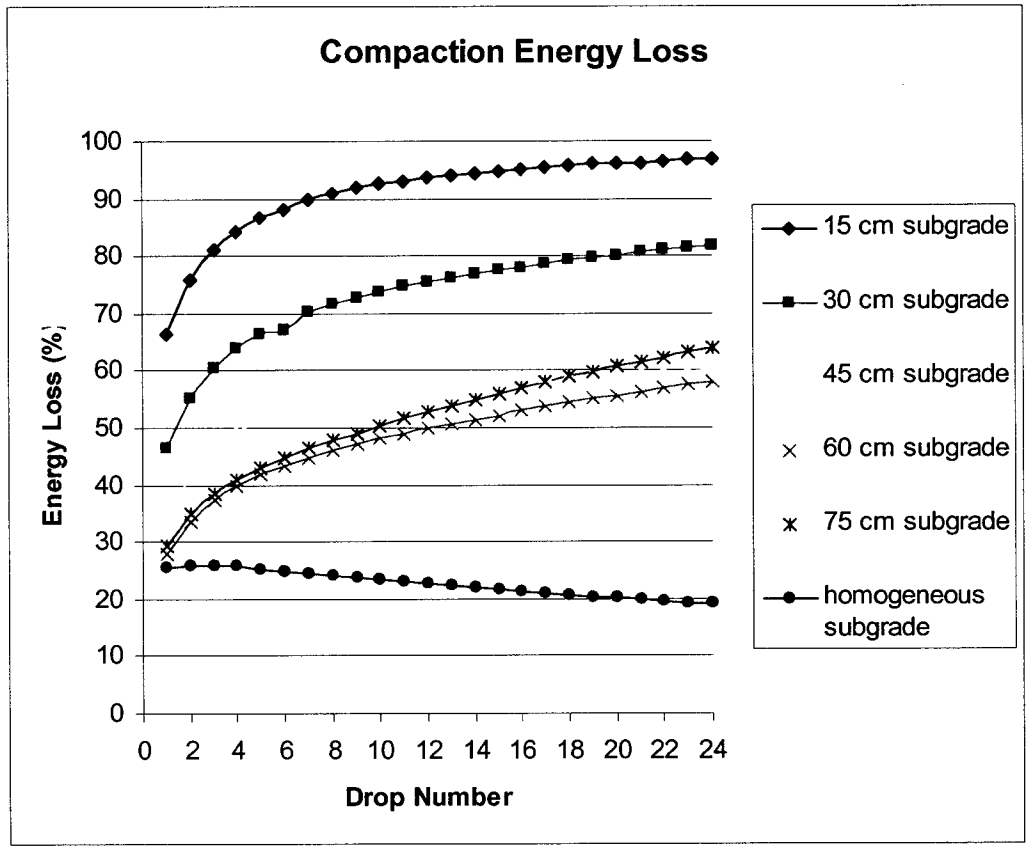

Figure 4.15: Calculated loss of compaction energies over time for weak lower layer (E_2=2500 kN/m^2)

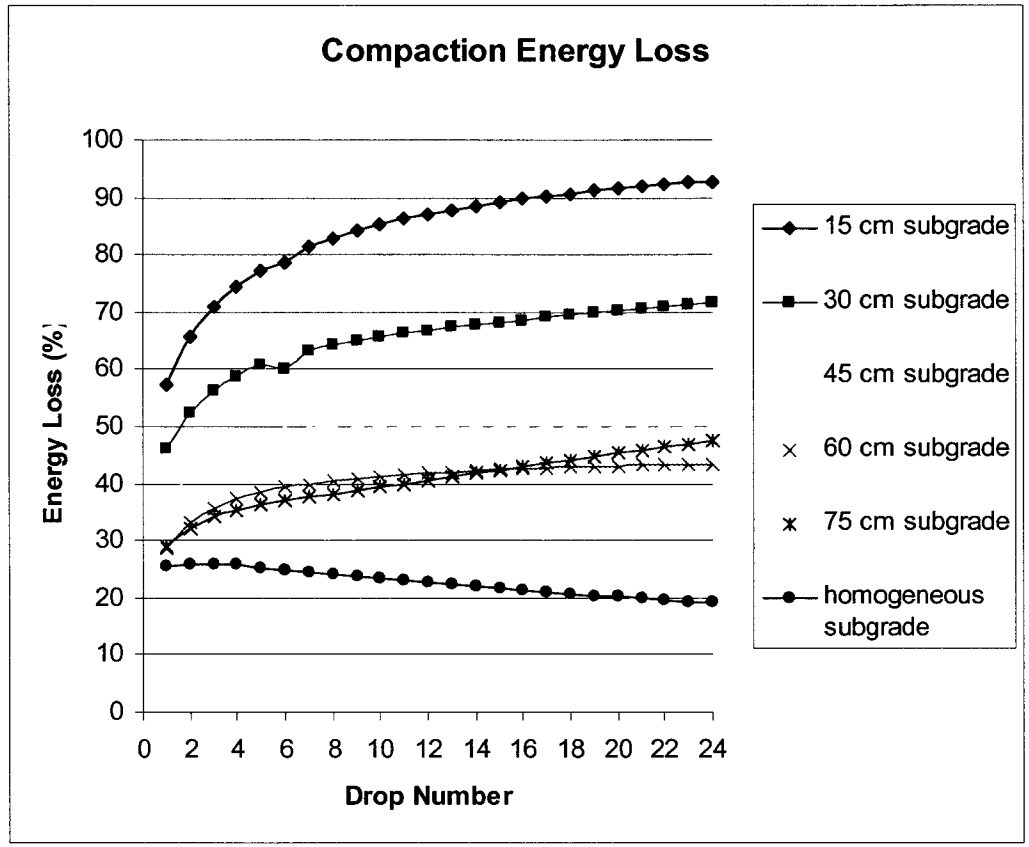

Figure 4.16: Calculated loss of compaction energies over time for weak lower layer (E_2=5000 kN/m^2)

From the results presented and figures 4.15 and 4.16, following conclusions can be withdrawn:

a) The compaction energy loss over time in a two-layer system, where the lower layer is weak, is a time-dependant and non-linear mechanism in which the rate of the amount of energy lost to the lower layer is increasing as the compaction process is continued.

b) On the contrary to the statement above, energy loss due to lack of confinement for a homogenous subgrade is almost a stable process, the loss of energy being around 20 % of the applied energy.

c) For the worst case scenario, where the subgrade is underlain by a weak deposit with its depth being equal to the target depth of compaction, over 90-95 % of the compaction is done in the weak lower layer after 24 drops with increasing energy loss to the lower layer.

d) When the subgrade to be compacted is underlain by a weak deposit, after a certain period of time in compaction process, the compaction will start to be done only in the weak lower layer resulting in no additional compaction in the subgrade. It can be seen from the figures above that the loss in compaction energy is reaching 100 % asymptotically as the energy is

continued to be applied. After that point on, the subgrade will be punched to the lower layer resembling an elevator moving downwards.

e) The exact time or the number of drops after which the subgrade will reach its maximum achievable compaction depends on the depth of the subgrade and stiffness of the lower layer. As the lower layer stiffness and the subgrade depth are increased, it will take longer for the compaction to be done only in the lower layer, resulting in a better compaction in the subgrade.

4.10 DESIGN RECOMMENDATIONS

Upon the results taken from the analyses, the following recommendations can be made:

a. In case of a weak lower layer, lower energy levels must be used in order to achieve compaction. It was already shown that lower energy values gave relatively less amounts of compaction energy loss to the lower layer. In that regard, the λ coefficient to calculate the amount energy per drop value should be taken in the range of 0.6 to 0.7 that correspond to two lower energy levels used in this study. Therefore, it is more reliable and convenient to use a lower amount of energy per drop with higher number of drops to increase the attainable compaction level.

b. The depth of the subgrade layer will also play an important role on the achievable level of compaction in a way that it will increase the thickness of the "buffer zone" between the subgrade and the lower layer material and reduce the energy seepage.

c. With respect to the statement above, the depth of the subgrade layer in a compaction project should be taken at least three times the depth of target improvement depth as it was found to be the critical depth.

d. For an ongoing compaction process, after the subgrade depth reaches 5 times the target depth of improvement, it is possible to achieve proctor compaction values

by applying proper amount of energy. Since the lower layer will not be sensed after this depth for the subgrade and considering that the previous layers are compacted to some extent, the energy level may be increased to speed up the compaction process.

4.11 ESTIMATION OF COMPACTION LEVEL

The correlation between the percentage of energy loss to the stiffness of the lower layer and the depth of subgrade was already shown in the first part of numerical results. Coefficients a, b, and c were introduced, that would enable the calculation of energy loss percentage for stiffness levels used in this study for different depths of subgrade.

For practicing engineers, these coefficients for specific stiffness levels of the lower layer will be presented by means of design charts, which will make it possible to find values of these coefficients for different stiffness levels of the lower layer. The charts for coefficients a, b, and c are shown as figure 4.17, 4.18, and 4.19.

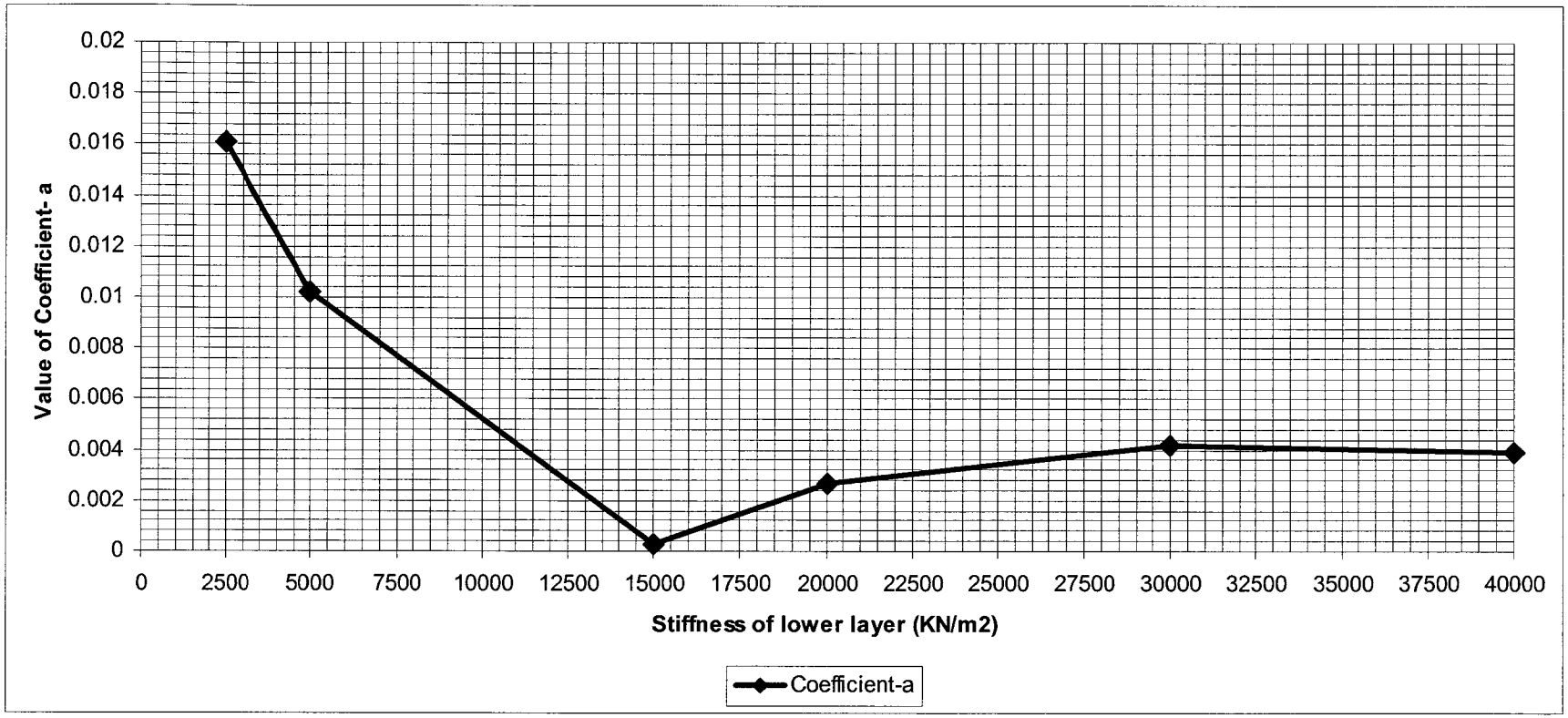

Figure 4.17: Values of Coefficient-a for different stiffness levels of the lower layer

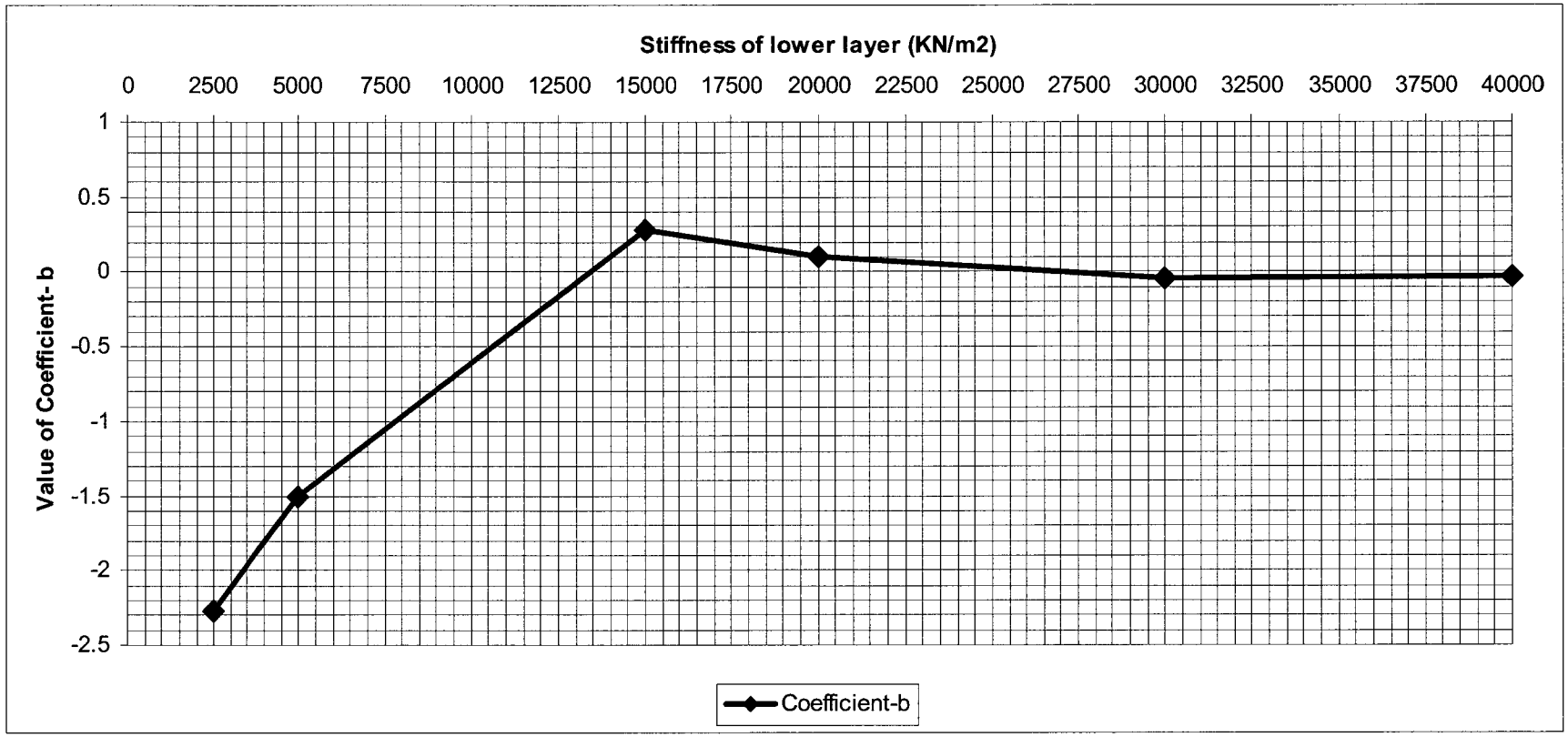

Figure 4.18: Values of Coefficient-b for different stiffness levels of the lower layer

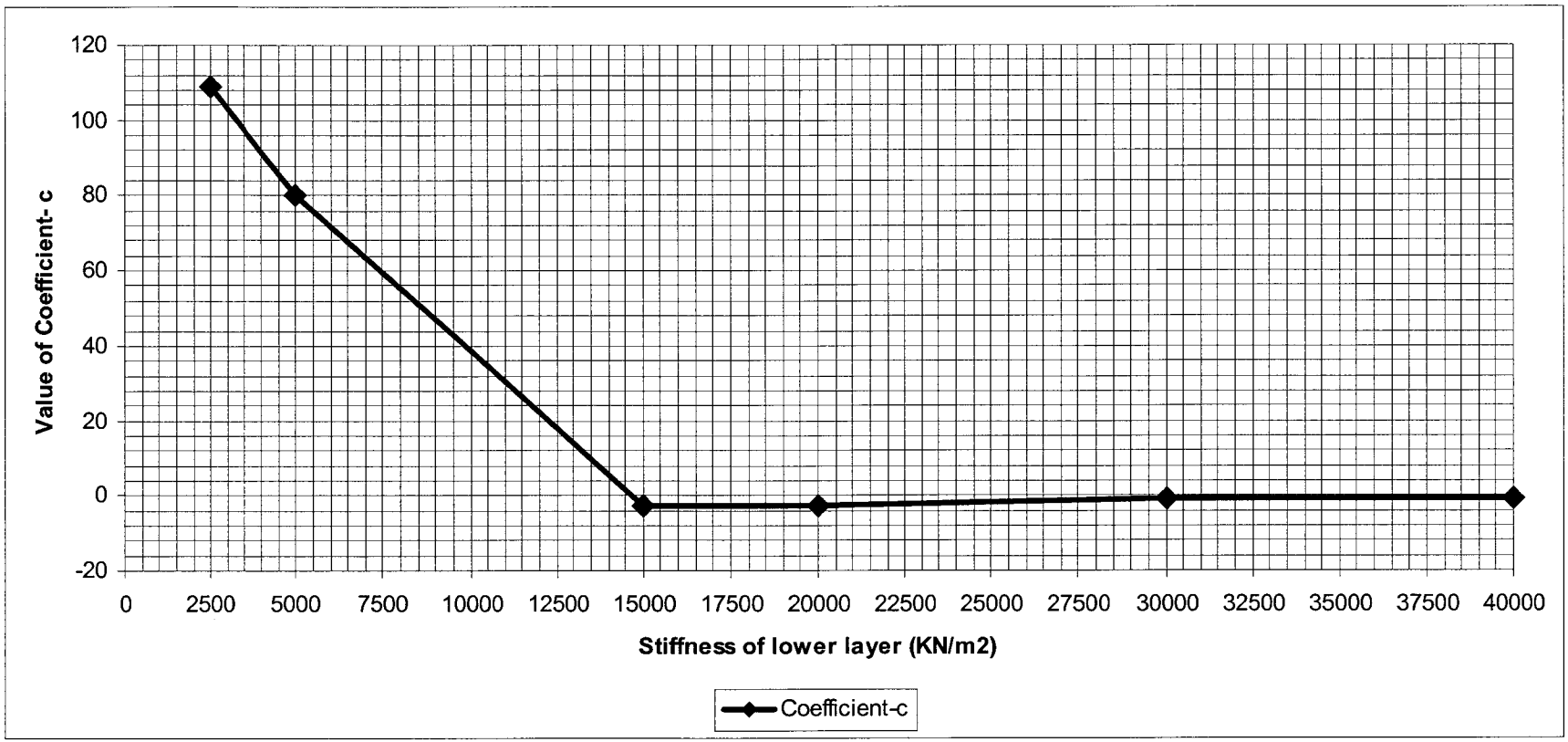

Figure 4.19: Values of Coefficient-c for different stiffness levels of the lower layer

For practical purposes, an energy-based compaction approach will be employed to convert the amount of energy loss to the proctor compaction achieved for the subgrade. For this purpose, achieved compaction level after a certain amount of energy input will be taken as a function of load-settlement behavior of the subgrade. That is to say, the load-settlement curve will be approximated as an "energy-compaction achieved" curve, in which there will be no more compaction after a certain amount of energy that is trapped by the subgrade. This compaction level will be taken as 95% proctor compaction, and will coincide with the maximum settlement value on the load-settlement curve for the homogenous subgrade. Hence, figure 4.14 will be switched to "energy-compaction achieved" curve as shown in figure 4.20. The compaction level of subgrade after 24 drops will be taken as 80% compaction since approximately 20% of equivalent proctor compaction energy was found to dissipate to the lower layer. Subsequently, the characteristic curve will be extended up to 95% compaction and a relation between the energy trapped by subgrade and the achieved compaction level will be obtained.

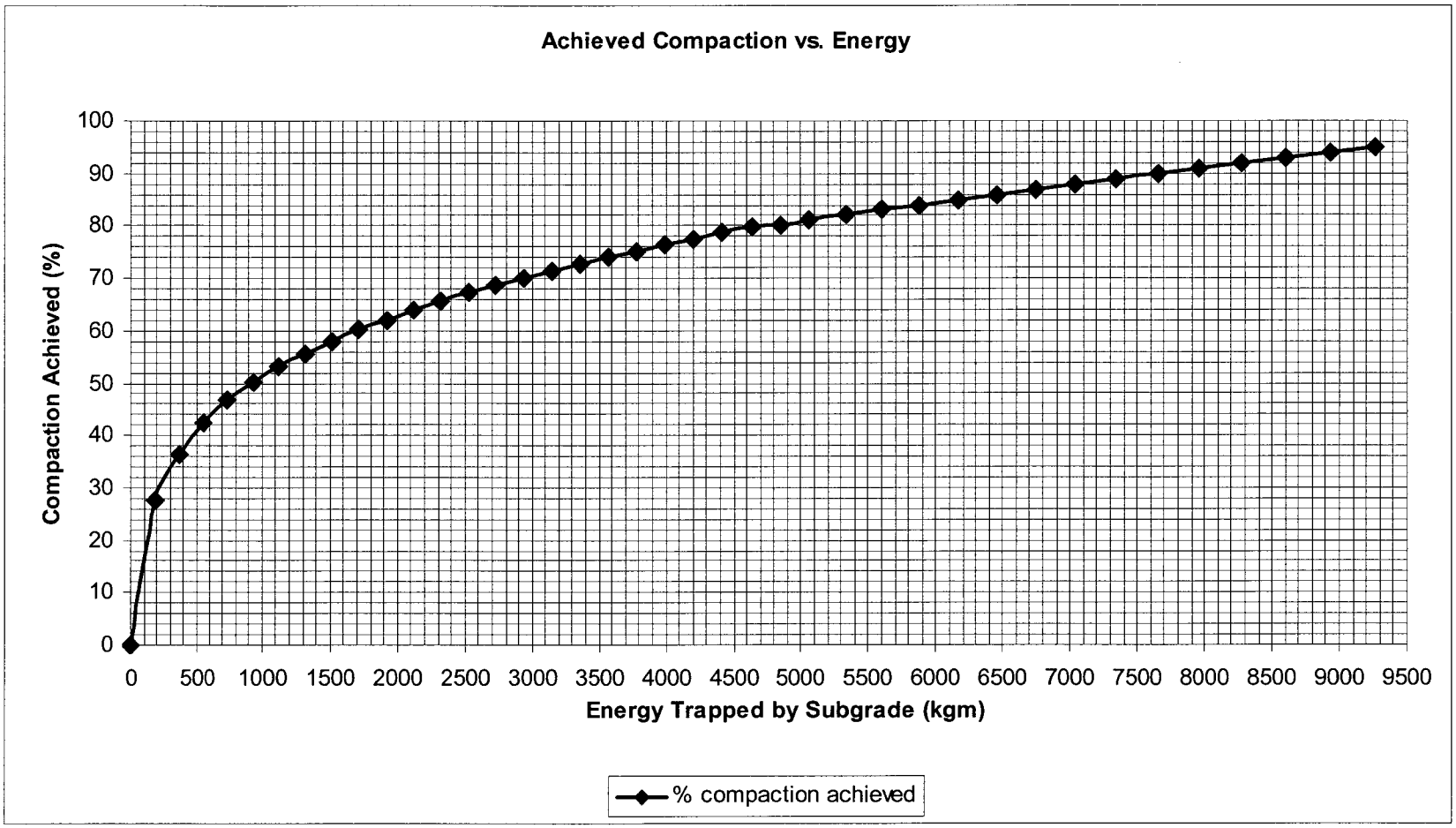

Figure 4.20: Achieved Compaction Levels in the Subgrade with respect to Energy Trapped

For an accurate evaluation of the compaction achieved in the subgrade, the percentage of compaction will be converted to the dry density of subgrade, in which 95% proctor compaction will equal the 95% maximum dry density obtained in Proctor Test. On the other hand, the initial dry density of subgrade before compaction will be taken as point 0 on compaction percentage values. Therefore, the dry density at any level of compaction will be:

$$\gamma_{dry} = \gamma_{initial} + \frac{(95\%\gamma_{proctor}) - (\gamma_{initial})}{100} \times (Compaction\%) \quad \text{..... (4.4)}$$

In conclusion, the dry density at any level of compaction with respect to the depth of subgrade and stiffness of the lower layer can be approximated by formula 4.4. In order to predict the energy dissipation to the lower layer and relative dry density of subgrade at any stage of compaction, a flow diagram is given that takes all design considerations and coefficients into account following a step-by-step procedure.

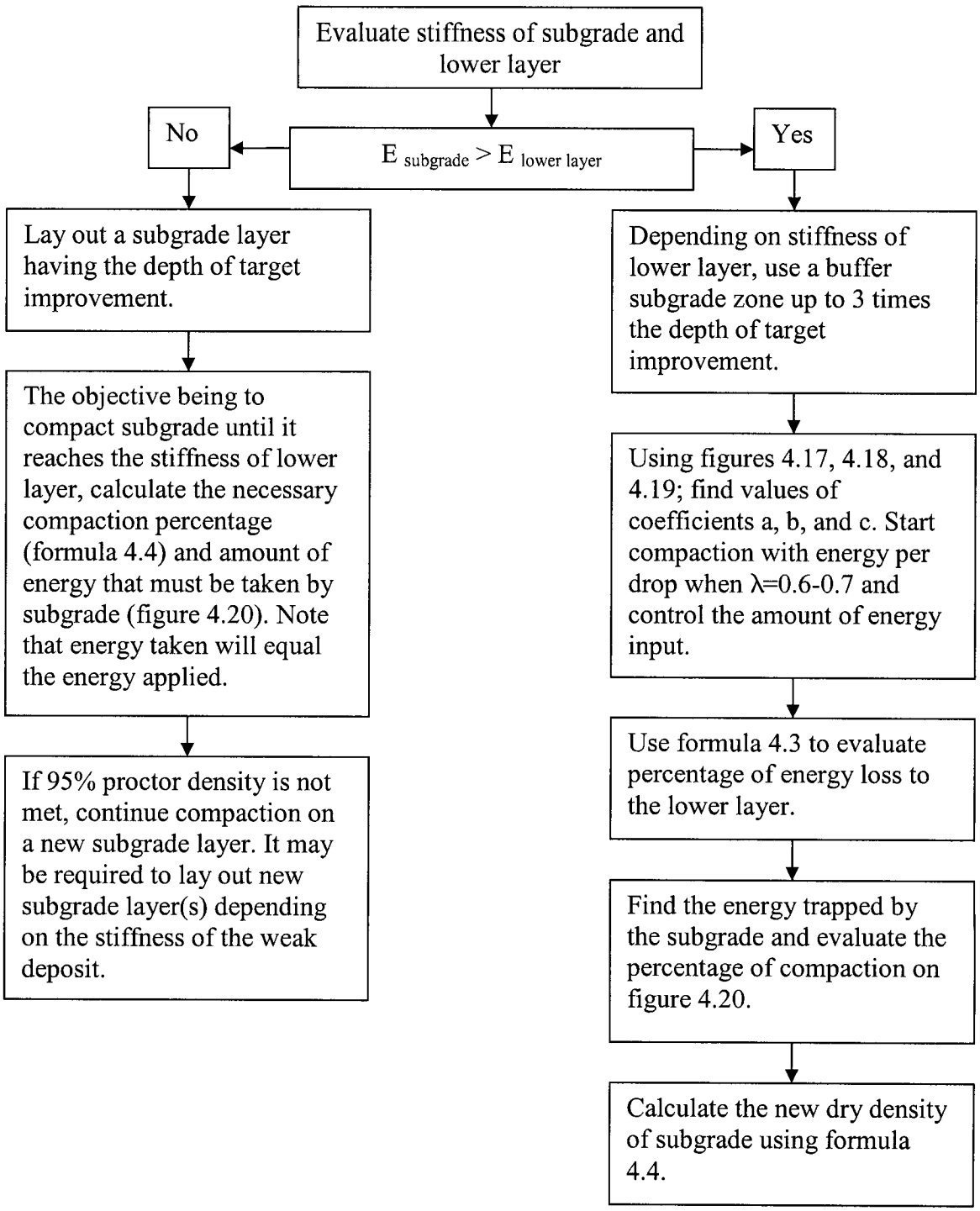
Evaluate stiffness of subgrade and lower layer
$E_{subgrade} > E_{lower\ layer}$
No
Yes
Lay out a subgrade layer having the depth of target improvement.
The objective being to compact subgrade until it reaches the stiffness of lower layer, calculate the necessary compaction percentage (formula 4.4) and amount of energy that must be taken by subgrade (figure 4.20). Note that energy taken will equal the energy applied.
If 95% proctor density is not met, continue compaction on a new subgrade layer. It may be required to lay out new subgrade layer(s) depending on the stiffness of the weak deposit.
Depending on stiffness of lower layer, use a buffer subgrade zone up to 3 times the depth of target improvement.
Using figures 4.17, 4.18, and 4.19; find values of coefficients a, b, and c. Start compaction with energy per drop when λ=0.6-0.7 and control the amount of energy input.
Use formula 4.3 to evaluate percentage of energy loss to the lower layer.
Find the energy trapped by the subgrade and evaluate the percentage of compaction on figure 4.20.
Calculate the new dry density of subgrade using formula 4.4.

CHAPTER 5

CONLUSIONS

5.1 GENERAL

An axisymmetric numerical model was developed utilizing the Finite Element Technique to simulate Dynamic Compaction of a thin subgrade layer overlying deep deposit. Dynamic analyses of the two-layer system were performed with successive drops on the ground executed through a transient load in the form of a sine-wave. The following can be reported:

1. Proctor Test is not suitable for predicting field compaction. This is due to lack of compatibility of the boundary conditions between the laboratory and the field compaction.

2. The parameters governing the compaction of a subgrade layer are the stiffness of the lower deposit, thickness of the subgrade, and the energy level used.

3. Level of compaction of a subgrade layer increases due to the increase of the depth of subgrade and energy applied. In that regard, application of compaction with lower energy per drop values (λ=0.6-0.7) and higher number of drops will increase the densification achieved in the field.

4. The energy dissipation to the lower deposit after the repeat of impact load was found to be crucial; in some cases it is impossible to compact the subgrade as the deposit absorb all of the energy applied, causing the subgrade layer to sink through the deposit.

5. It has been found that, reasonable values for Rayleigh Material Damping coefficients can be obtained by incorporating expected frequency levels of generated vibrations in a soil deposit and the ratio of Dynamic Shear Modulus to Maximum Shear Modulus with anticipated strain levels upon loading. This approach can be studied in further research and the parameters may be used as the in-situ Material Damping parameters in design of Machine Foundations, Numerical Analyses to evaluate Liquefaction Potential and simulating Dynamic Compaction.

6. The method used to evaluate the duration of loading and unloading for successive drops have also found to be proper for numerical analyses that require the simulation of impact loading on the ground. The analytical approach using the conservation of momentum and a triangular dynamic force-time response upon impact reasonably predicted peak dynamic stress with respect to the energy level. Thus, the formulation can be used in the field of Dynamic Compaction of Soils to predict tamper settlement values or assess general dynamic soil behavior after each drop for all types of soils whose Elastic parameters (E and ν) are known.

7. Design charts and a step-by-step design procedure are provided for practicing use. The design procedure will enable engineers to predict the achievable compaction level of the

subgrade overlying a deposit of known stiffness. Moreover, design recommendations are given to choose the proper energy level and the thickness of the subgrade layer to be used.

As an alternative to design recommendations and procedure provided, precautions can be taken in advance to avoid poor compaction of subgrade layers. If the lower layer is relatively weak, improvement of this layer may be taken into consideration by using injection method (cement, lime) before compaction is initiated. Using a geo-membrane layer would also be efficient in reducing the effect of the weak deposit. In the case of organic material or a layer of contaminated soil comprising the deposit, it would be inevitable to remove the soil and replace it with granular material.

5.2 RECOMMENDATIONS

A laboratory and field modeling for the problem stated to validate the level of compaction, which can be achieved under given boundary conditions.

REFERENCES

Athanasopoulos, G. A., Pelekis, P. C., Anagnostopoulos, G. A., 2000, "Effect of Soil Stiffness in the attenuation of Rayleigh-wave motions from field measurements", Soil Dynamics and Earthquake Engineering, Vol. 19, pp. 277-288.

Das, B. M., 1996, Principles of Geotechnical Engineering, California State University, Sacramento, USA.

Das. B. M., 1993, Principles of Soil Dynamics, Southern Illinois University at Carbondale.

Hanna, A. M., 2003, "Laboratory Compaction of a Subgrade Layer Overlying a Deep Soil Deposit", Ground Improvement, Vol. 7, No. 1, pp. 1-8.

Ishabashi, I. and Zhang, X., 1993, "Unified Dynamic Shear Moduli and Damping Ratios of Sand and Clay", Soils and Foundations, Vol. 33, No. 1, pp. 182-191.

Pan J.L and Selby, A.R. 2002, "Simulation of Dynamic Compaction of Loose Granular Soils", Advances in Engineering Software, Vol. 33, pp. 631-640.

Lee, F. H. and Gu, Q., 2004, "Method for Estimating Dynamic Compaction Effect on Sand", Journal of Geotechnical and Geoenvironmental Engineering, Vol. 130, No. 2, pp. 139-152.

Lukas, R. G., 1980, "Densification of Loose Deposits by Pounding", Journal of the Geotechnical Engineering Division, Proceedings of the American Society of Civil Engineers, Vol. 106, No. GT4.

Mayne, P. W. and Jones, J. S. Jr., 1983, "Impact Stresses During Dynamic Compaction", Journal of Geotechnical Engineering, Vol. 109, No. 10

Mayne, P. W., 1985, Ground Vibrations During Dynamic Compaction, Vibration Problems in Geotechnical Engineering, Edited by George Gazetas and Ernest T. Selig, Proceedings of a Symposium sponsored by the Geotechnical Engineering Division in conjunction with the ASCE Convention in Detroit, Michigan.

Mayne, P. W., Jones, J. S. Jr., Dumas, J. C., 1984, "Ground Response to Dynamic Compaction", Journal of Geotechnical Engineering, Vol. 110, No. 6.

Poran, C. J. and Rodriguez, J. A., 1992, "Design of Dynamic Compaction", Canadian Geotechnical Journal, Vol. 29, pp 796-802.

Poran, C., Heh, K., Rodriguez, J.A., 1992, "Impact Behavior of Sand", Japanese Society of Soil Mechanics and Foundation Engineering, Soils and Foundations, Vol. 32, No. 4, pp. 81-92.

Poran, J. P. and Rodriguez, A. J., 1992, "Finite Element Analysis of Impact Behavior of Sand", Japanese Society of Soil Mechanics and Foundation Engineering, Soils and Foundations, Vol. 32, No. 4, pp. 68-80.

Scolombe, B. C., 1993, "Ground Improvement, Dynamic Compaction", Edited by Moseley, M. P., Hayward Baker Inc., Maryland, USA.

Welsh, J. P., 1987, "Soil Improvement- A Ten Year Update", Proceedings of a Symposium sponsored by the Committee on Placement and Improvement of Soils of the Geotechnical Engineering Division of the American Society of Civil Engineers in conjunction with the ASCE Convention in Atlantic City, New Jersey, Geotechnical Special Publication No. 12.

Y.K. Chow, D.M. Yong and S.L. Lee, 1990, "Monitoring of Dynamic Compaction by Deceleration Measurements", Computers and Geotechnics, Vol. 10, pp 189-209.

Zerwer, A., Cascante, G., and Hutchinson, J., 2002, "Parameter Estimation in Finite Element Simulations of Rayleigh Waves", Journal of Geotechnical and Geoenvironmental Engineering, Vol. 128, No. 3, pp 250-261.